Building and Environment 186 (2020) 107293

Contents lists available at ScienceDirect

Building and Environment

journal homepage: http://www.elsevier.com/locate/buildenv

A numerical study of the impact of vegetation on mean and turbulence fields in a European-city neighbourhood

Francesco Barbano [a,b], Silvana Di Sabatino [a], Rob Stoll [b], Eric R. Pardyjak [b,*]

[a] University of Bologna, Department of Physics and Astronomy, Bologna, 40126, Italy
[b] University of Utah, Department of Mechanical Engineering, Salt Lake City, UT, 84112, USA

ARTICLE INFO

Keywords:
Urban street canyon
Vegetation
Sustainability
QUIC Dispersion Modeling System
Simplified computational fluid dynamics

ABSTRACT

Vegetation in the urban environment has various impacts on microclimate. While optimal strategies for investigating these impacts are the subject of ongoing research, most approach rely on Computational Fluid Dynamics (CFD) simulations. We evaluate mean wind and turbulence fields simulated using the fast-running Quick Urban & Industrial Complex (QUIC) Dispersion Modeling System, a simplified CFD tool that resolves buildings and vegetation. We use QUIC to investigate the role of deciduous trees in modifying the airflow of a real neighbourhood in Bologna, Italy by running large ensembles of simulations per case study, obtained by varying the input wind direction. This approach can minimise intrinsic model uncertainty as well as uncertainties associated with real environments. Model validation is performed using measurements from an experimental field campaign focused on a vegetated urban street canyon in Bologna. Ensemble simulation results show good agreement with the experimental data for various conditions (i.e., simulation ensembles overlap experimental variability in most cases). The role of trees is investigated by comparing simulations with and without trees. Trees are found to reduce airflow by constraining local circulation and reducing turbulence intensity. Finally, the combined effect of building morphology and vegetation is investigated by adopting a formalism to represent the presence of vegetation using area-fraction coefficients. An area-fraction coefficient threshold of 0.225 has been identified that separates flow behaviours and is present in cases with and without vegetation. Below this threshold, a constant wind and turbulence regime exists, while above the threshold, winds and turbulence vary with area-fraction coefficient.

1. Introduction

Investigations of urban 'breathability' have contributed to a vigorous interest in understanding the impacts of vegetation on the flow and turbulence fields in cities. During the last two decades, different approaches have been used to tackle the problem, mostly involving numerical investigations. Many papers have concluded that vegetation in urban environments exerts a drag force that reduces the flow-field intensity by causing a net loss of momentum [1–4], with a consequent modification of both production (transfer from the mean flow) and destruction (eddy fragmentation leading to dissipation) of the turbulence [1,5,7–9,59]. As a consequence of these modifications, scalar transport and mass removal are affected, which have implications on air quality [10–12] and thermal comfort [6,13] in the urban environment. Vegetation also leads to the enhancement of particle deposition [4,7,14] and resuspension [15,16], crown transpiration [17], and shadowing effects [18].

Numerical investigations addressing vegetation impacts on urban environments are usually addressed using Large-Eddy Simulations (LES) and Reynolds Averaged Navier-Stokes Simulations (RANS). These Computational Fluid Dynamics (CFD) approaches ensure a realistic representation of the flow dynamics in complex environments (e.g. vegetated urban canopies) and yield high-resolution flow fields. Nevertheless, it is not common to perform numerical simulations of real environments due to the lack of measurements necessary for model validation. A few examples can be found in the literature that address the ability of CFD models to reproduce the urban environment of compact cities that are typical in Europe. Among those [3,18], used a RANS model to simulate the atmospheric flow field in the city of Lecce in southern Italy. They concluded that a significant windbreak effect can be observed in street canyons with trees. While the trees have minimal impact on wind patterns, they significantly reduce the magnitude of

* Corresponding author. University of Utah 1495 East 100 South, Room 1550 MEK, Salt Lake City, UT, 84112, USA.
E-mail addresses: francesco.barbano3@unibo.it (F. Barbano), pardyjak@eng.utah.edu (E.R. Pardyjak).

https://doi.org/10.1016/j.buildenv.2020.107293
Received 23 June 2020; Received in revised form 27 August 2020; Accepted 10 September 2020
Available online 23 September 2020

wind speeds, indicating that the presence of trees is important when studying ventilation and dispersion problems. A hybrid model (RANS coupled with an external urban vegetation module) was adopted by Ref. [19] to simulate the flow field in two neighbourhoods of Lisbon and Aveiro, Portugal. Their work highlighted the fundamental impact of vegetation on pollutant dispersion for different incident wind directions relative to a street canyon [4,20]. used a RANS model to reproduce the flow and dispersion fields in the neighborhoods of Marylebone (London, UK) and Pamplona (Spain) respectively, concluding that the aerodynamic effects of trees are more important at lower wind speeds and for parallel wind direction to the streets, causing a weaker ventilation and little turbulent dispersion especially below the vegetation canopy. Among LES studies [21], simulated the turbulent flow field in a neighbourhood of Vancouver, Canada. They showed that trees in canopies act as a mean-flow momentum sink and reduce turbulent transport of high-momentum flux.

These examples show recent applications of CFD models to real environments with vegetation. However, these types of CFD models are associated with large computational costs limiting their applicability to practical (e.g., design) or nowcasting applications. Moreover, trees are considered porous media and their impacts are parametrised as source/sink terms (a viscous term and an inertial loss term) in the fundamental equations [22], developed based on laboratory investigations. Most common parametrisation methods imply the use of a pressure loss coefficient as inertial loss term [23] or that of a momentum sink in the Navier-Stokes equations given by the vegetation foliage drag on the atmospheric flow [24]. In the first method, vegetation has no effect on turbulence production nor dissipation, while in the second method vegetation converts mean flow kinetic energy into wake turbulence (turbulence source term) or dissipates turbulence energy at length scales smaller than those generated by shear. As for the momentum sink, these source/sink contributions are inserted as additional terms in the turbulence kinetic energy and turbulence dissipation rate equations (for a more exhaustive review on the argument, the reader is referred to Ref. [22].

In this study, a 'simplified CFD' approach is tested on a real vegetated urban environment using the Quick Urban & Industrial Complex (QUIC) Dispersion Modeling System [25]. QUIC is a fast-response model that is able to compute 3D flows, turbulence, and particle dispersion around explicitly resolved buildings and trees by combining a mass-conserving wind solver with a mixing-length turbulence model and a Lagrangian random-walk particle transport model [25–28]. QUIC does not solve the full Navier-Stokes equations. Instead, QUIC specifies quasi-steady state velocities everywhere in the domain based on empirical parametrisations as an 'initial-guess' wind field. This initial wind field is then forced to be mass consistent using a variational analysis technique, which builds on the work of [29,30]. This methodology produces reliable results and at a significantly reduced computational costs without loosing domain resolution. This type of framework allows vegetation volumes (single vegetation elements or entire canopies) to be modelled using idealised solutions such as the exponential solution proposed by Ref. [31]; and thus avoids further parametrisation within the Navier-Stokes equation, as done in most CFD models. Because QUIC is fast, it can be used to conduct investigations based on ensemble simulations (not just a single realisation). Performing multiple simulations with small changes to the input conditions can minimise both boundary-condition uncertainty and intrinsic model uncertainties.

In this paper, we evaluate the performance of the QUIC model and further assess the impact of urban morphology on the mean flow and turbulence fields. The simulation's results are validated with measurements collected during a field campaign (summer 2017) carried out in the city of Bologna (44° 29' N, 11° 20' E, 56 m above means sea level), Italy, as part of the European funded H2020 iSCAPE (Improving the Smart Control of Air Pollution in Europe) project (https://www.iscapeproject.eu/). The validation aims to prove the efficacy of a fast-running simplified model to characterise the canopy-layer dynamics and the impact of vegetation. The primary motivation is to understand the usefulness of a fast-response CFD solver, and what are its limits in a densely built-up real urban environment. Moreover, this study provides a first-time evaluation of QUIC's turbulence model in a real urban environment.

The paper is structured as follows. After this introduction, the methodology section (Sect. 2) focuses on QUIC's setup and on a short description of the experimental field campaign, providing the investigated domain and measured data for validation. Section 3 focuses on the validation of the simulated results among the measured data, evaluating QUIC performance for different wind direction conditions. Section 4 investigates the impact of vegetation on the mean flow and turbulent fields, focusing on the effects of a morphology modification imposed by a different vegetation amount. Finally, Sect. 5 presents a number of conclusions.

2. Modeling methodology

In this study, we use the QUIC Dispersion Modeling System (version 6.1) to address the role of vegetation in modifying the mean flow and turbulence fields of a real urban neighbourhood. While QUIC has been discussed extensively elsewhere [25,26,28,32], we present a brief review of the relevant aspects of the modeling methodology here. QUIC is a fast-response model that combines a mass-conserving wind solver (QUIC-URB) with a Lagrangian random-walk dispersion model (QUIC-PLUME). As discussed in the introduction, QUIC-URB does not solve the Navier-Stokes equations. Instead, QUIC uses a set of empirical parametrisations to compute an initial 3D wind velocity field $\boldsymbol{u}_0=(u_0\hat{i} + v_0\hat{j} + w_0\hat{k})$ in regions of complex morphology [28]. Specifically, simple algebraic expressions are used to specify winds occurring in regions of complex flow around buildings such as the upstream recirculation region, the near and far wakes, rooftop recirculation regions, and street canyon flow regimes. A variational technique is then used to enforce mass-conservation. The final, divergence-free wind field $\boldsymbol{u}_f=(u_f\hat{i} + v_f\hat{j} + w_f\hat{k})$ is obtained by minimising the variance of the difference between the initial and the final wind fields. The details of QUIC's wind-field solver are presented in Ref. [28].

QUIC-PLUME is an urbanised (i.e., modified for urban flows) Lagrangian random-walk model that calculates 3D turbulence and concentration fields from mean winds provided by QUIC-URB [26,32]. In this paper, we do not present any dispersion modeling results, however we evaluate QUIC-PLUME's turbulence model using field data. Hence, we only present a brief description of QUIC's turbulence model and do not discuss the random-walk model. Like QUIC-URB, QUIC-PLUME's turbulence model is broken up into three discrete regimes to simplify and speed up computations. In the regions away from buildings, the turbulence is governed by surface-layer similarity theory with boundary-layer height modifications. In addition, this regime has modifications for stability that are based on a user-prescribed Monin-Obukhov length scale. The second regime is designed to modify flow near surfaces and is based on simple mixing-length turbulence theory and local-gradient closure. In this regime, the local Reynolds stress is computed as $(l_{mix}/\varphi_m)(\partial U/\partial \boldsymbol{r})_{max}$, where l_{mix} is the mixing length scale, φ_m is the Monin-Obukhov stability function, U is the magnitude of the total wind speed, and r is the direction that yields the largest velocity gradient [33]. The mixing length is either computed from the shortest distance to a wall (d_{wall}) as $l_{mix} = kd_{wall}$ or as a mixing length related to the velocity magnitude and shear, namely, $l_{mix} = kU/|\partial U/\partial r|$, whichever length scale is smallest. We note that k is the von Kármán constant. The final regime accounts for enhanced non-local mixing due to sweeping eddies present in building recirculation zones. That is, accounts for high-momentum fluid outside of recirculation zones that is transported into the wake regions. In these regions, a non-local turbulence model is used to compute the Reynolds stresses that is based on length scales associated with the wake cavity and velocity magnitude

differences between the flow outside of the wake and within the wake. For a more exhaustive description of QUIC's turbulence modeling framework the reader is referred to Ref. [26,33].

QUIC's mean wind and concentration fields have been shown to compare well with traditional CFD models [34–36] and reliably represent both idealised [26,28] and real urban environments [25,37–40]. The current study offers the opportunity to test QUIC on a European city (Bologna, Italy) whose morphology is different from a typical North American city [41]. Furthermore, for the first time, QUIC's turbulence model is evaluated for a full-scale city test case. The core of European cities is their historical centre characterised by a dense network of narrow street canyons only interrupted by occasional squares or junctions. The surrounding suburban areas are typically arranged in residential and often vegetated neighbourhoods. Herein, QUIC simulations are verified using field measurements collected in Bologna, Italy, as part of the European funded H2020 iSCAPE project.

2.1. Experimental field campaign

Measurements collected in Bologna were part of a field campaign conducted during summer 2017 (August 07, 2017–September 26, 2017). The focus of the campaign was the characterisation of ventilation and thermal processes in a vegetated street canyon with the aim of generalising the results to any European residential vegetated neighbourhood [42]. The street canyon of Laura Bassi St. was chosen as a representative observation site (see Fig. 1). Laura Bassi St. is a two-lane 700-m long road, surrounded by a nearly regular arrangement of deciduous trees facing small private houses (2 floors) or apartments (3–5 floors), with a mean building height of 17 m. Despite being only a two-lane road, the presence of a private garden increases the mean canyon width to 25 m, yielding a mean aspect ratio of 0.7. Its orientation is north-south at a displacement angle of 24° from north. Being a residential area, the road is open to private vehicular traffic as well as some minor bus routes. The neighbourhood is a network of roads with similar dimensions and building characteristics. The majority of the street and neighbourhood vegetation is composed of deciduous trees belonging to the *Platanus Acerifolia Mil* family, a hybrid of *Platanus Orientalis* and *Platanus Occidentalis* types, widely found in urban European habitats. The average height of the branch-free trunk is 5 m and the ellipsoidal shaped crown extends up to 15 m, with a minor radius of 5 m. Along the street, trunks are regularly spaced by approximately 8 m, allowing a small amount of crown superposition. The composition of buildings and vegetation leads to a mean height H of the neighbourhood of 11 m.

Laura Bassi St. was fully instrumented to assess atmospheric dynamics, thermodynamics and turbulence. For the scope of this work, only the instrumentation needed for ventilation analysis are presented. Fig. 1 displays the locations of the instrumentation in the street. The thought-bubble colours highlight each level where the measurement stations were deployed: green refers to the rooftop (site LB3, 44° 28' 59.9'' N, 11° 22' 01.2'' E), red to the mid-canyon (site LB2, 44° 28' 54.6'' N, 11° 22' 00.4'' E) and blue to the ground (site LB1, 44° 29' 02.4'' N, 11° 22' 05.3'' E). The LB1 station was placed on the east side of the road beneath the tree crown at 3 m a.g.l.; the LB2 station protruded from a balcony toward the road at 9 m a.g.l., remaining in the small cavity between the building and the tree line; the LB3 station was located above a flat rooftop at 20 m a.g.l. (see Fig. 2).

Each level inside the canyon was equipped with a sonic anemometer (Windmaster 3D, Gill, Lymington, Hampshire, UK) sampling at 20 Hz, coupled with a thermohygrometer (HC2S3-L, Campbell Scientific, Logan, Utah, USA) sampling at 1 Hz. Site LB3 was instead equipped with an Young 81000 (RM Young Company, Traverse City, Michigan, USA) sampling at 10 Hz, and a CNR4 (Kipp & Zonen, Delft, Netherlands) net radiometer for measuring incoming and outgoing radiation components every 60 s. These stations facilitate the computation of both mean flow and turbulence quantities necessary for assessing ventilation processes within the street canyon and in the overlying roughness layer. Supporting meteorological data were retrieved from two meteorological stations belonging to the Emilia-Romagna Environmental Protection Agency ARPAE permanent network. They were located within the city and are representative of the roughness and the inertial layers respectively. The first station, named Silvani (site SI1, 44° 30' 03.9'' N, 11° 19' 42.6'' E), is located on top of a tall building at the edge of the city centre at a height of 40 m (a.g.l.). It is equipped with a cup and vane anemometer (WMS301, Väisälä, Helsinki, Finland) and a thermohygrometer (HMP230, Väisälä, Helsinki, Finland). The second is on top of the Asinelli Tower (site AS1, 44° 29' 39.2'' N, 11° 20' 48.2'' E) at the very centre of the city, at a height of approximately 100 m (a.g.l.),[1] equipped with a cup and vane anemometer (Vv20 adn Dv20, CAE, Bologna, Italy) and a thermohygrometer (THS, CAE, Bologna, Italy). The experimental setup was completed with a ceilometer (CL-31, Väisälä, Helsinki, Finland) located within the city centre (site CL1, 44° 29' 58.1'' N, 11° 21' 14.4'' E) that measured the boundary-layer height every 16 s. Data were preprocessed by first checking for non-physical data or instrumental fails [43] and then by applying reliability thresholds based on typical local ranges. Wind velocity components are considered reliable when $|(u,v,w)| \leq 20$ m s^{-1}, while for sonic and air temperature the applied threshold is $|T| \leq 50$ °C. Sonic data were then despiked following the [44] method; the time series was divided into small intervals (5 min as suggested by Ref. [45] which are expected to follow a Gaussian distribution. In each interval, spikes are defined as values larger than 3.5 times the standard deviation of the distribution [46] and replaced by the interval mean, evaluated without the spikes. Finally, wind velocity components were rotated along the streamline direction [47] so that speed $\left|\overrightarrow{U}\right| \approx (u,0,0)$. As the typical slope angle of the neighbourhood terrain is smaller than 1°, no slopes have been considered.

2.2. QUIC setup

The neighbourhood in Fig. 1 is also used as the domain for the QUIC simulations. The domain size is $x = 1000$ m, $y = 1300$ m and $z = 200$ m, with a fixed horizontal resolution ($\Delta x, \Delta y = 2$ m) and the vertical Δz increases exponentially with the height z by a factor 0.15 from the surface value $\Delta z_s = 1$ m. The total number of cells in the domain was 3.25×10^6. The computations were run (via a FORTRAN executable) on a single processor of a 4.0 GHz Intel core i7 workstation. This resulted in a processing and data-writing time (for both QUIC-URB and QUIC-PLUME) of approximately 10 min, 70% of which is occupied by the data writing. Since no wind profiles were available within or nearby the city to be used as input, a logarithmic profile is imposed as the input for QUIC-URB:

$$U(z) = \frac{U_{ref}\left(ln\left((z+z_0)/z_0\right) + \Psi(z/L)\right)}{ln\left(\left(z_{ref}+z_0\right)/z_0\right)}, \tag{1}$$

where U_{ref} is the user-input reference velocity at the height z_{ref}, z_0 is the aerodynamic roughness length, L is the Obukhov length and $\Psi(z/L)$ is the stability correction function. A logarithmic profile in Eq. (1) was selected from experience working with the model, which indicates that the log profile yields better solutions inside the canopy with respect to the urban canopy input profile, as the urban canopy profile tends to underestimate the velocity field within the canopy layer. Reference velocity and height are retrieved from the SI1 station. The aerodynamic roughness length z_0 is computed following [49] and modified according to Refs. [50] to account for the presence of vegetation. The Obukhov

[1] The height of this measurement site is reported as 92 m when comparing simulation results and measurements, as the shapefile used for QUIC's domain tends to underestimate the real height of unconventional buildings such as Asinelli Tower, a historical slightly-leaning tower.

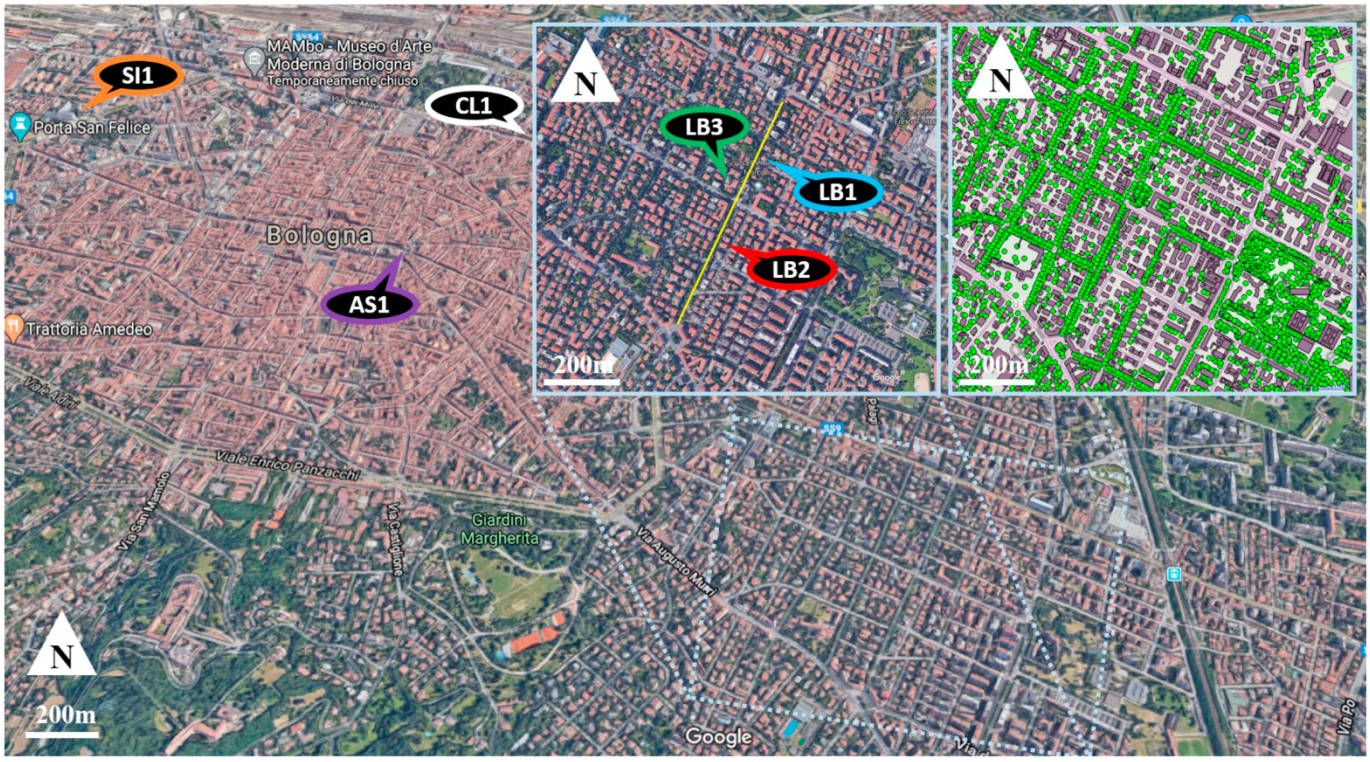

Fig. 1. Top view of Bologna. The panels highlight the domain of the investigation, i.e. the neighbourhood of Laura Bassi St. (on the left) and its representation in QUIC (on the right). The yellow line indicates the street canyon, while the coloured thought bubbles indicate the locations of the measurement stations in Laura Bassi St. (LB1 in blue, LB2 in red and LB3 in green) and at the supporting sites (AS1 in purple, SI1 in orange and CL1 in white). (Source: https://www.google.com/maps). (For interpretation of the references to colour in this figure legend, the reader is referred to the Web version of this article.)

Fig. 2. Measurement sites within Laura Bassi St. during the experimental field campaign in Bologna. Acronyms and colours identify the locations on Fig. 1. (For interpretation of the references to colour in this figure legend, the reader is referred to the Web version of this article.)

length L is estimated at the top of the canyon. A summary of the model input parameters, domain dimensions and selected solving algorithms is given in Table 1.

QUIC-PLUME needs input values to compute realistic turbulence quantities. Reference surface temperatures are retrieved from the LB1 thermohygrometers deployed in the streets. Reference air temperature and humidity are taken from the ARPAE meteorological station. Finally, the boundary-layer height is retrieved from the ceilometer measurements in CL1.

2.2.1. Vegetation modeling approach

As mentioned in Sect. 2.1, the *Platanus Acerifolia Mil* tree family represents the vast majority of vegetation in the domain. This is the only vegetative type considered in the QUIC simulations. Vegetation is approximated as a porous obstacle, interpreted as a vegetated canopy even if it is composed of a single isolated tree. The empirical parametrisation for the initial wind-speed profile within a vegetated canopy uses the analytical solution proposed by [31].

$$U(z) = U_{h_v} \exp a\left(\frac{z}{h_v} - 1\right), \tag{2}$$

Table 1
Setup configuration for the QUIC simulations.

Algorithm/Parameter	Type/Value
Rooftop surfaces roughness (z_0)	0.1 m [48]
Street canyon algorithm	Rockle with Fackrell cavity length (Gowardhan et al., 2010; [58] Hayati et al., 2019)
Wake algorithm	Modified Rockled
Blended region algorithm	On (Gowardhan et al., 2010; [48]
Rooftop algorithm	Recirculation (Gowardhan et al., 2010; [48]
Upwind cavity algorithm	High-rise MVP model (Gowardhan et al., 2010; Hayati et al., 2019)
Side wall algorithm	On (Hayati et al., 2017)
Non-local mixing algorithm	On (Williams et al., 2004)
Domain size	1000 m × 1300 m × 200 m
Resolution	2 m × 2 m × 1 m (exponential in z)

where $U(z)$ is the horizontal wind speed at height z, U_{h_v} is the horizontal wind speed at the vegetation mean height h_v and a is the attenuation coefficient associated with specific types of roughness [51]. In order for Eq. (2) to be a reliable solution for the wind speed inside a vegetation element, the following variables are assumed as constant over the vegetation height: the foliage drag coefficient, the leaf area density function and the foliage shelter factor for momentum [27]. In the current analysis, all trees are approximated by porous cylinders of constant height $h_v = 15$ m and diameter $d_v = 5$ m. Within these volumes, the wind speed is given by Eq. (2), with h_v and a as input parameters, and U_{h_v} matching the velocity profile in Eq. (2) with the displaced-wall log-law wind-speed profile above the canopy [27]. The attenuation coefficient is calculated from measured data as in Ref. [51] by solving Eq. (2) for a:

$$a = \frac{ln\left(\overline{U}(z)\Big/\overline{U}_H\right)}{z/H - 1}. \tag{3}$$

As the closest measurement to the tree top is collected at LB3, h_v is set equal to H so that $U_{h_v} = \overline{U}_H$, the wind speed at H averaged over the considered time period. $\overline{U}(z)$ is the mean wind speed measured at LB1 and LB2 over the considered time period. Following this method, $a = (1.7 \pm 0.3)$. Compared with [51]; the computed attenuation coefficient value is closer to crop fields than tree canopies, which have smaller coefficients depending on the tree type. On the other hand, it could be misleading to rely only on this comparison to check the reliability of the coefficient value since [51] results were obtained for homogeneous vegetative canopies. To check the reliability of the evaluated coefficient, we used a to compute the vegetative drag coefficient C_v, which we then compared with recent literature results (e.g. Ref. [4] suggesting a $C_v = 0.25$ for Platanus trees in agreement with [18]. To accomplish the task, we performed a simple simulation where a single tree was placed in an empty domain. The aim is to calculate the area between the wind-speed profile within the tree and the unperturbed input profile. This area represents the total drag force F exerted by the tree on the unperturbed flow. Using a finite difference method, the vertical variation in drag force, $\Delta F(z)$, was calculated from velocity profiles. From the drag force, the drag coefficient C_v was computed as

$$C_v = \sum_z \frac{2\Delta F(z)}{\rho A_f^v U(z)^2}, \tag{4}$$

where ρ is the air density, A_f^v is the tree frontal area and U is the input velocity profile. From the attenuation coefficient evaluated with Eq. (3), the retrieved vegetative drag coefficient using Eq. (4) is $C_v = (0.24 \pm 0.4)$ in agreement with literature values. The result provides confidence in the attenuation coefficient computation method and will also be used for the further analysis. First, C_v is used to evaluate the porosity of the tree crown $P = (1 - C_v/1.08)^{1/1.8} = (0.56 \pm 0.05)$, as defined by Ref. [52]. Then, they are both be used in the following section to calculate the area density coefficients.

Turbulence fluxes are also important within vegetation. The turbulent kinematic momentum flux $\overline{w'u'}$ is modelled using a mixing-length closure, so that

$$-\overline{w'u'} = l^2 \left|\frac{\partial U}{\partial z}\right|^2, \tag{5}$$

where l is the mixing length, whose value is taken as a function of the height within the canopy [27]. In the lower part of the canopy ($z/h_v < 0.3$), $l = kz$ ($k = 0.4$ is the von Karman constant) following [31]. In the upper part of the canopy ($z/h_v \geq 0.3$), $l \propto a^{-1}$ following [53].

2.2.2. Area density coefficients

To compute the aerodynamic roughness length z_0, a set of coefficients must be extracted from the domain. Frontal (λ_f) and planar (λ_p) area fraction coefficients have been computed following [49]. However, the presence of vegetation must be included as a supplementary areal contribution. Therefore, we explicitly add the vegetation contribution term to the building contribution in the frontal (A_f) and planar (A_p) areas, as introduced by Ref. [50]:

$$A_f = A_f^b + P_v A_f^v, \tag{6a}$$

$$A_p = A_p^b + (1 - P) A_p^v. \tag{6b}$$

The superscript b indicates the building area and v the vegetation area. P_v is defined by Ref. [50] as the ratio between the vegetation C_v and the building drag coefficient C_b. P is the crown porosity evaluated as described in Sect. 2.2.1.

The building drag coefficient C_b is taken as unity in agreement with previous studies on European cities [41,54]. The vegetative drag coefficient is derived as explained in Sect. 2.2.1 using Eq. (4). Total and building planar areas are directly extracted from the QUIC simulation domain. The building frontal area is defined as

$$A_f^b = \sum_i \frac{h_i \cdot l_i \cdot \Delta_j}{\overline{\Delta}}, \tag{7}$$

where h_i is the height of the i^{th} building in the domain, l_i is the width of the i^{th} building under the assumption that all buildings have square facades, Δ is the domain length in the direction of the approaching input wind and $\overline{\Delta}$ is the mean domain length. The subscript j indicates the specified approach wind direction used in the model.

The square facade assumption for computing l is necessary since the only information on building facades is the total area, from which it is impossible to retrieve the shape. However, the normalised domain length $\Delta/\overline{\Delta}$ smooths the uncertainty in A_f adding or removing a compensating factor due to the different lengths of the domain along x and y axes. Therefore, A_f^b changes with the input wind direction, but maintains the same value for opposite winds (e.g. north and south, east and west). Conversely, A_f^v is not wind-direction dependent due to the frontal symmetry of the trees associated with their approximated shape (Sect. 2.2.1). Therefore, it is defined as

$$A_f^v = h_v \cdot d_v \cdot n, \tag{8}$$

where h_v is the tree height, d_v is the crown diameter and n is the number of trees in the domain. $h_v \cdot d_v$ represents the maximum cross-section of the single tree. Inserting Eqs. (7) and (8) into Eq. (6a), the frontal area is evaluated for the whole domain.

The vegetative planar area is simply defined as the cylinder base area (assumed shape of the tree) multiplied by the total number of trees in the

domain:

$$A_p^v = \pi \cdot r^2 \cdot n. \quad (9)$$

Substituting Eq. (9) and the values for A_p^b retrieved directly from the domain into Eq. (6b), the planar area is evaluated for the domain. Planar λ_p and frontal λ_f area fraction coefficients are then evaluated as A_p / A_t and A_f / A_t, respectively. Note that both vegetative areas in Eqs. (8) and (9) are null in absence of vegetation, in which case the area fraction coefficients become equal to classical ones from Ref. [49]. Areas and coefficients values are reported in Table 2 together with the aerodynamic roughness length z_0 and the displacement height d, computed from the area fraction coefficients as described in Ref. [49]; considering both cases of the neighbourhood with and without the presence of vegetation.

2.2.3. Local friction velocity correction

The computation of turbulence in QUIC is driven by locally computed friction velocities, u_*. Moreover, u_* is needed to evaluate the wind-velocity fluctuations for the Lagrangian random-walk dispersion component of the model. The correct computation of the friction velocity is therefore fundamental when investigating turbulence, which is central to this study. To fix an inconsistency in QUIC version 6.1, we introduced a new routine to calculate u_*. As previously introduced in Sect. 2, the computation of the initial flow field relies on a set of empirical parametrisations that are algebraic formulas for the 3D velocity field in several regions of the domain such as recirculation zones, building wake regions, cavities (i.e. the parametrised regions). Within QUIC, the friction velocity is computed as the sum of local (u_*^{loc}) and non-local ($u_*^{non-loc}$) terms, respectively describing the local mixing related to the atmospheric flow and the non-local mixing resulting from the interactions between the flow and the obstacles [26]. While the non-local term is well represented by version 6.1 of the code, at the floor of the urban canopy surface (i.e., the first grid point above the ground) outside the parametrised regions u_*^{loc} is calculated by inverting the law-of-the-wall velocity profile, using an iterative method which should ensure that the friction velocity is constant along a vertical profile. This method fails when the wind-speed profile is largely non-logarithmic. The major limitations of this technique are: (i) the a-priori assumption of a logarithmic shape of the mass conserved wind-speed profile and (ii) the divergence of the iteration technique if u_*^{loc} is not a constant. As a result, u_* converges to unrealistic values.

To overcome this issue, we applied a simple code fix to at the first grid points above the ground outside the parametrised regions when the a-priori assumption fails, i.e. when the iterations diverge, to recompute u_*^{loc} using the finite difference version of the log-law wind-speed profile as

$$u_*^{loc} = k(z_1 + z_0)\frac{\Delta U}{\Delta z} \Big/ \varphi(z_1 / L), \quad (10)$$

where $k = 0.4$ is the Von Karman constant, z_1 is the first grid point above a surface which is not involved in any of the previously described parametrisations, z_0 is the aerodynamic roughness length, $\Delta U/\Delta z$ is the wind speed vertical gradient computed at each grid point of the non-parametrised regions within the first layer above the surface and $\varphi(z_1 / L)$ the stability function. The strength of this computation is that a value of u_*^{loc} is associated with the mass conserved unperturbed flow, without addressing the shape of the wind profile. For a more exhaustive description of the procedure used to fix this error and its validation on a simple geometry, we refer the reader to Ref. [55].

Table 2
Setup quantities Laura Bassi domains. Between brackets is reported the input wind direction considered (when important).

Quantity	With vegetation	Without vegetation
A_t	1300000 m^2	1300000 m^2
A_p	271808 m^2	261798 m^2
A_f	329478 m^2 (N-S)	259240 m^2 (N-S)
	407249 m^2 (E-W)	337011 m^2 (E-W)
λ_p	0.21	0.20
λ_f	0.25 (N-S)	0.20 (N-S)
	0.31 (E-W)	0.26 (E-W)
d	4.65 m	4.51 m
z_0	1.51 m (N-S)	1.26 m (N-S)
	1.75 m (E-W)	1.5 m (E-W)

3. QUIC validation

To investigate the role of vegetation in real urban neighbourhoods, we simulate the profiles of wind speed (U), turbulence kinetic energy (TKE), and kinematic momentum flux ($|\overline{w'u'}|$) and compare them to measured data within and above the Laura Bassi St. canyon. To perform the model validation using measurements and to further investigate the role of vegetation, we use a novel method suitable for the fast-responding nature of QUIC. In this method, wind-direction ensembles (multiple simulations) are performed without changing any other input parameters. The validation is performed for four different wind-direction ensembles with respect to the canyon orientation, namely east-west ('canyon perpendicular') and north-south ('canyon parallel'). Each wind-direction ensemble is defined as an envelope of ±20° around each cardinal compass point with a simulation run every 5°, for a total of 9 simulations per ensemble. Similarly, wind directions measured at LB3 are considered constant if the direction angle lies between ±20° of the cardinal point. The ±20° direction interval is chosen since it includes the measured wind-direction variability (i.e. the complete range) within the investigated periods. Four intervals of constant wind direction are retrieved from measured data, each of them lasting an hour. Input parameters and comparative quantities are averaged over each period to enhance the validation robustness. We simulate a profile per quantity at each canyon site, since their locations are horizontally displaced. We also attempt to simulate the mean behaviour of each quantity in the canyon by calculating the profiles at the canyon centre and comparing them with all the canyon sites (and the supporting sites when dealing with wind speed). Each simulated profile is calculated from a horizontal average of a few cells around the location of the measurement stations. The following common inputs are used in each ensemble: (i) the reference velocity to compute the input logarithmic profile, using Eq. (1), is retrieved from SI1 site, at a reference height $z_{ref} = 40$ m; (ii) the vegetation attenuation coefficient is calculated from Eq. (3) and is set at $a = 1.7$. It is also worth mentioning that measurements at site LB3 are taken directly above a building rooftop, and so the profiles are cut at the building height.

3.1. East perpendicular

Fig. 3 shows the simulated ensemble profiles for the east-perpendicular wind directions wd ($70° \leq wd \leq 110°$) from the 22:00–23:00 UTC+2 (local time) time period of the September 20, 2017, compared with measured data from each measurement site within and above the canyon. The reference wind speed for the input logarithmic profile is $U_{ref} = 2.0$ m s^{-1}. The aerodynamic roughness length is set at $z_0 = 1.75$ m according to Table 2, while the Obukhov length is calculated at LB3 and its inverse is $1/L = 0$ m^{-1}. An atmospheric profile of temperature and relative humidity was retrieved from the thermo-hygrometer's data at each level within the canopy and the urban boundary layers. The atmosphere was isothermal with $T = 288.4$ K. There were small oscillations in the relative humidity around the input value $RH = 60\%$. The boundary-layer height ($h_{BL} = 480$ m) was still decreasing toward typical nocturnal values.

Reasonable agreement is found between the simulated profiles and

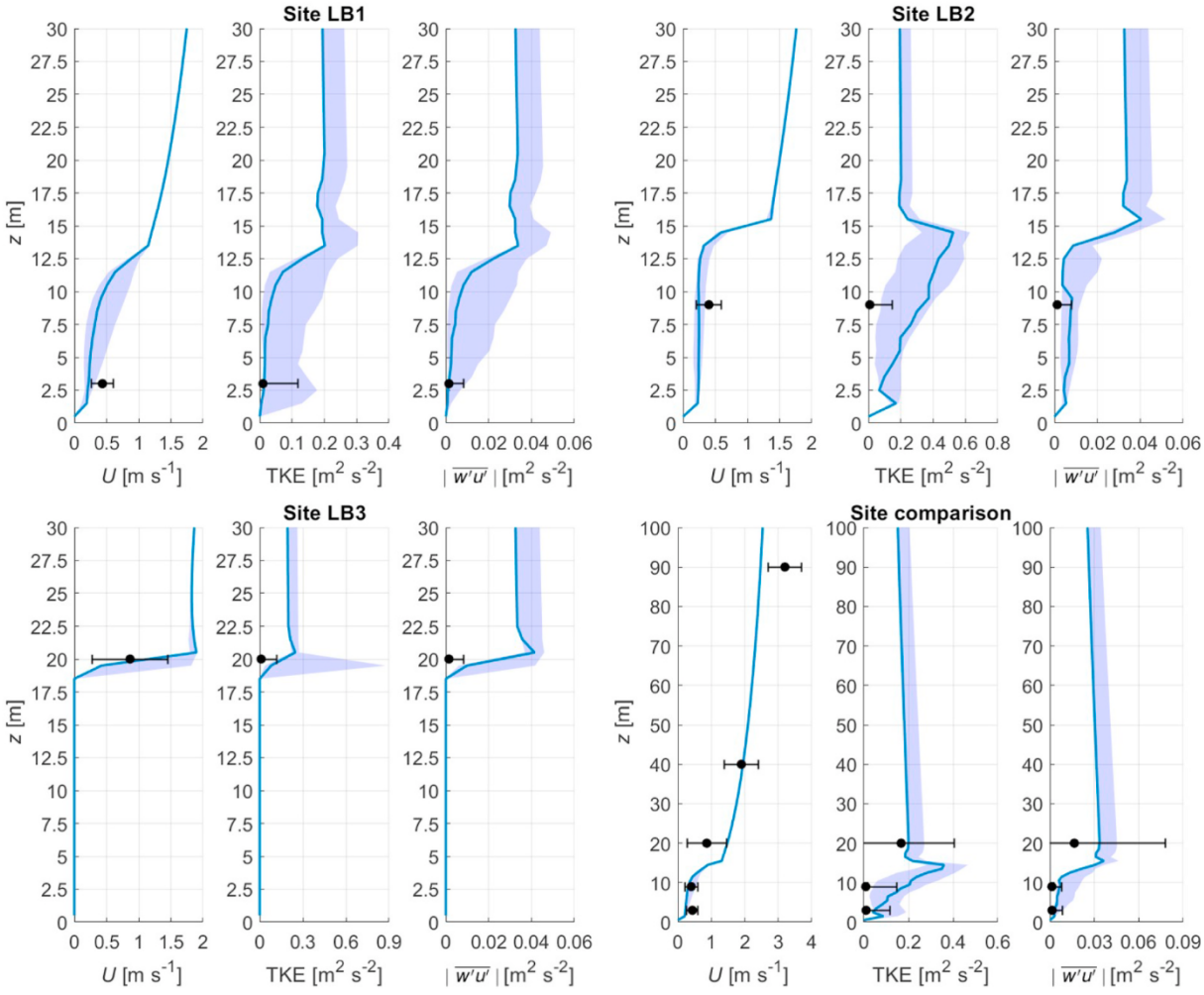

Fig. 3. Profiles of simulated and measured wind speed U, turbulence kinetic energy TKE, and kinematic momentum flux $|\overline{w'u'}|$ at LB1 (top left), LB2 (top right) and LB3 (bottom left) sites within Laura Bassi St. for the easterly perpendicular wind direction ensemble. A sites comparison is also given (bottom right), where the wind speed is also compared to SI1 ($z = 40$ m) and AS1 ($z = 100$ m) measurements. The blue profile represents the case with the wind direction 90° to the canyon orientation, while the shaded area is the complete range of the wind direction ensemble. The black dots and error bars refer to the observed means and standard deviations within the selected period. (For interpretation of the references to colour in this figure legend, the reader is referred to the Web version of this article.)

the measured values for wind speed and both turbulence-related quantities. Within the canyon, the wind speed is underestimated by the model, but still within the measurement error bars. This underestimation could result from the model inability to capture the acceleration due to reduced flow volume between the tree crown and the surface (at LB1) or the building facade details (at LB2). Turbulence kinetic energy and turbulent kinematic momentum flux are well captured at LB1, but slightly overestimated at LB2 and LB3 (as displayed in the bottom left panel of Fig. 3). Despite the good agreement for wind-speed values, turbulence is overestimated by the simulation as a result of a turbulent layer that does not exist in the measured data. Agreement is still good if a single representative profile is computed for the canyon (see the bottom right panel of Fig. 3). These profiles are not meant to match the data perfectly, but to assess how representative the measurements are of the flow behaviour. Poor agreement was expected inside the canopy, where local morphological features and the vicinity of trees can have a role in the modification of the profile. However, the agreement is good for both mean flow and turbulent quantities, confirming the results found at each measurement site. Wind speed is also compared to the SI1 and AS1 sites to assess the flow behaviour at larger scales. SI1 is very well simulated, verifying the logarithmic shape of the wind velocity profile outside the canopy layer. However, the wind speed at AS1 is poorly represented, due to the possible perturbation of the logarithmic profile by the larger-scale flow, which enhances the wind speed in the upper part of the urban boundary layer.

3.2. West perpendicular

Profiles simulated for the west-perpendicular wind-direction ensemble ($250° \leq wd \leq 290°$) are displayed in Fig. 4 for the interval 09:00–10:00 UTC+2 on September 21, 2017. The reference wind speed is $U_{ref} = 2.1$ m s^{-1}. As for the east-perpendicular case, $z_0 = 1.75$ m. The inverse Obukhov length was $1/L = -0.0242$ m^{-1}, or near-neutral stability. The measured temperature was isothermal inside the canopy ($T_c = 292$ K) and almost equal to the ambient temperature outside it ($T_a = 291$ K). Relative humidity ranged between $RH_c = 50\%$ in the canopy to $RH_a = 40\%$ above the canopy at AS1. The boundary layer was growing with a height of $h_{BL} = 750$ m.

Fig. 4 indicates that the agreement between the simulations and measurements is better than the east-perpendicular ensemble for most of the sites and quantities. All profiles are within the error bars of the measurements, (even the site comparison panel in Fig. 4, bottom right). However, a slight level of underestimation can be found inside the canopy (displayed in the top panel of Fig. 4) where both wind speed and kinematic momentum flux are smaller than the measurements. Again in the proximity of a boundary, such as at the ground or on a building

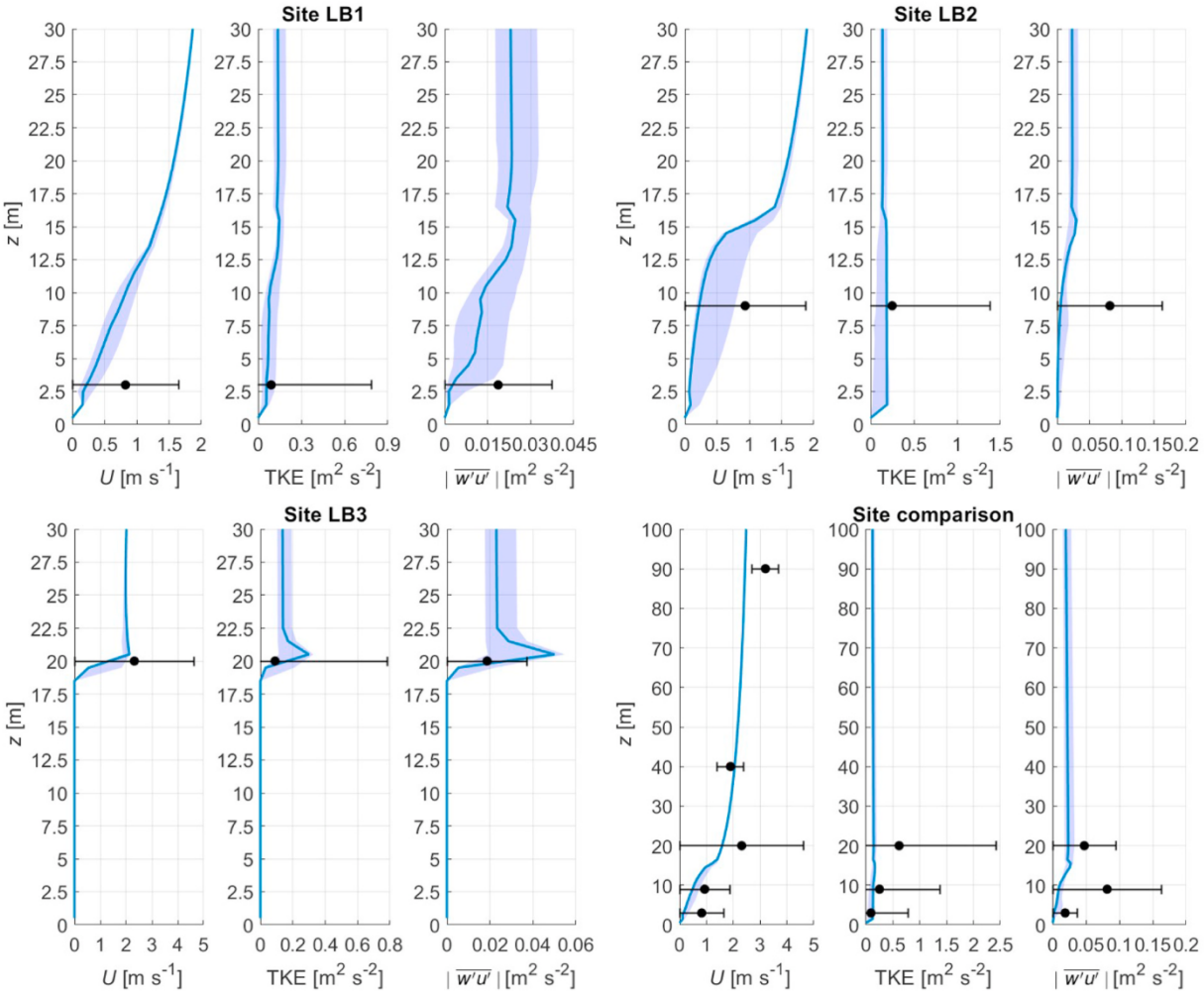

Fig. 4. Same as Fig. 3 but for the west perpendicular wind direction ensemble. The blue profile represents the 270° wind direction to the canyon orientation. (For interpretation of the references to colour in this figure legend, the reader is referred to the Web version of this article.)

facade, the model estimations are not as good, but still within the range of confidence of the data.

3.3. North parallel

The simulated profiles for the north-parallel wind-direction ensemble ($-20° \leq wd \leq 20°$) are shown in Fig. 5 for the period 16:00–17:00 UTC+2 on September 22, 2017 when the reference wind speed was $U_{ref} = 1.5$ m s^{-1}. The aerodynamic roughness length is $z_0 = 1.51$ m according to Table 2. The inverse of the Obukhov length ($1/L = -0.0223$ m^{-1}) indicates near-neutral stability. The in-canyon temperature ($T_c = 296$ K) was slightly larger than the ambient ($T_a = 295$ K), while relative humidity decreased from $RH_c = 43\%$ to $RH_a = 33\%$ from the canyon surface to AS1 station. The boundary-layer height ($h_{BL} = 1336$ m) is typical of daytime hours.

Turbulence kinetic energy and turbulent kinematic momentum fluxes obtained from the simulations overestimate the data from measurements. The measured wind speed is also underestimated at LB1 (as shown in the top left panel of Fig. 5) due to the poor representation of the flow acceleration between the tree crown and the surface. Conversely, wind speed is overestimated at LB2 (as displayed in the top right panel of Fig. 5). In both cases, the wind speed profiles are independent of the wind direction (the ensemble collapses on the cardinal point profile), as a consequence of flow channelling. The site-comparison profiles (shown in the bottom right panel of Fig. 5) overestimate the in-canopy turbulence as already observed at the measurement locations, and underestimate both mean flow and turbulence above the rooftop level.

3.4. South parallel

Fig. 6 shows simulated profiles for the south-parallel wind-direction ensemble ($160° \leq wd \leq 200°$) for the 03:00–04:00 UTC+2 time period on September 22, 2017. This last scenario presents some differences compared to those previously analysed. The reference wind speed is stronger ($U_{ref} = 5.3$ m s^{-1}) due to the possible development of a nocturnal jet at the city scale. A stable stratification, indicated by a $\Delta T = 2$ K is observed between 40 m and 100 m a.g.l., affects the urban boundary layer. However, air within the canopy and at the rooftop interface remains well mixed due to heat loss from the building facades. As a result, a weakly unstable condition develops inside the canyon ($1/L = -0.0816$ m^{-1}).

The relative humidity does not follow the temperature inversion and ranges between $RH_c = 69\%$ inside the canyon and $RH_a = 50\%$ at AS1. The observed boundary-layer height was $h_{BL} = 455$ m.

Simulated wind speed at the three canyon sites are in reasonably good agreement with the measured data. Turbulence-related quantities show peculiar profiles, with large magnitudes inside the canopy and a rapid decrease approximately at the height of LB2 where the temperature gradient becomes positive. At the canyon-centre (site comparison in Fig. 6, bottom right panel), the turbulence kinetic energy maximum is closer to the street surface, as already observed at LB1, while the

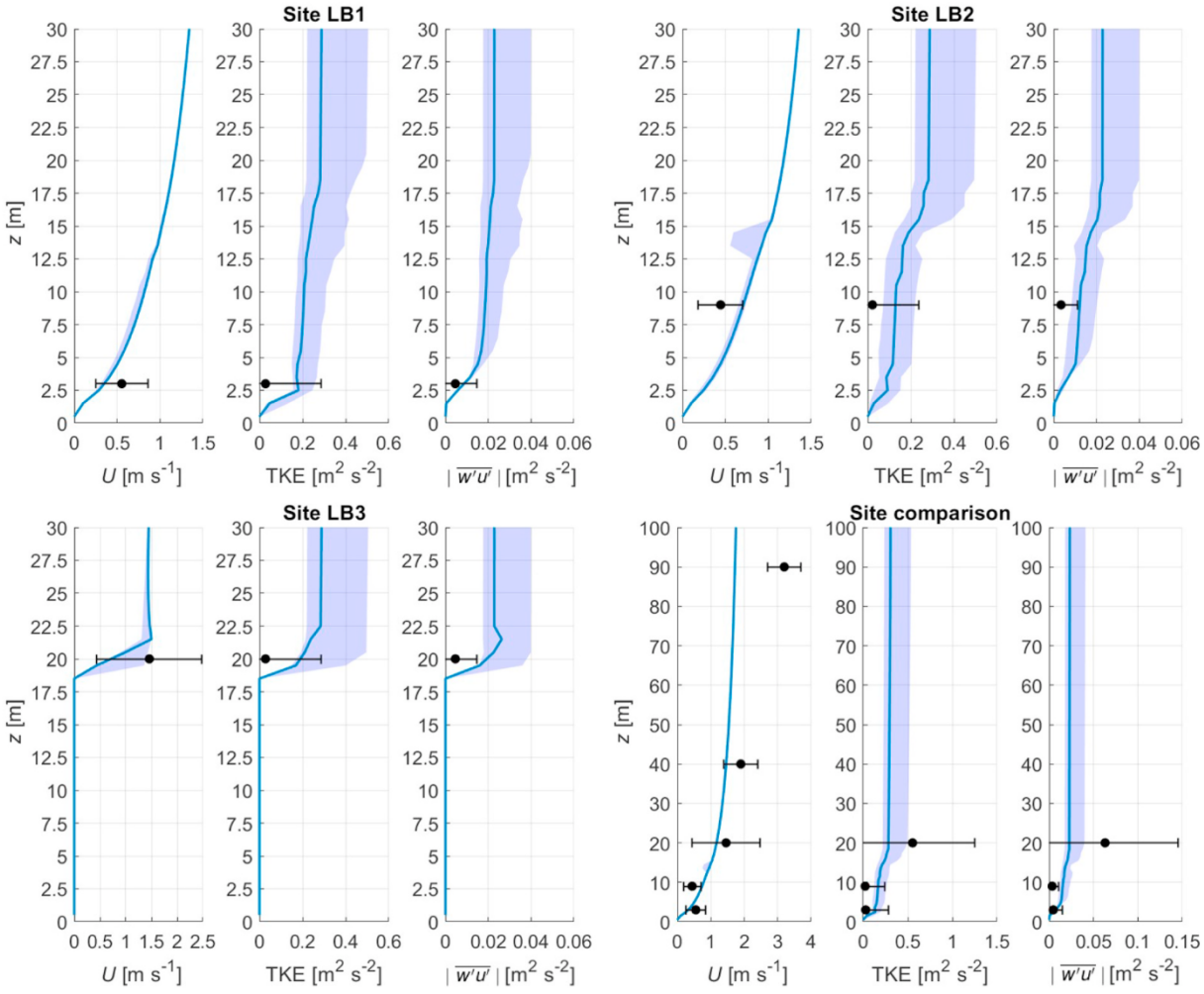

Fig. 5. Same as Fig. 3 but for the north parallel wind direction ensemble. The blue profile represents the 0° wind direction to the canyon orientation. (For interpretation of the references to colour in this figure legend, the reader is referred to the Web version of this article.)

momentum-flux maximum remains confined in the lower half of the canyon. Near the facades (LB2 site in Fig. 6, top right panel), turbulence maxima are retrieved close to the rooftop level, creating a small upper canyon circulation confined between the buildings and the trees. These differences in TKE behaviour at the LB1 and LB2 locations could be caused by differences in the local geometry of the canyon, which are larger at LB1 than at the LB2 height. In this case, the simulations always overestimate the field data. We speculate that this may be a result of the simultaneous complex superposition of unstable conditions within the canyon and stable stratification above that are not parametrised in the model.

4. Results

To investigate the role of vegetation, we compare two different cases, resulting from as many numerical simulations. The first, or 'Tree case', is the actual (high-density) tree cover in the neighbourhood. The second extreme is a vegetation-free scenario where the trees are removed called the 'No-Tree case'. The investigation is performed on the east-perpendicular wind-direction ensemble case (using the same ensemble of wind direction that was used to perform the validation), using the input parameters and wind profile described in Sect. 3.1 and Table 2.

To show the qualitative impact of vegetation on the flow and turbulence fields, a cross-section for each quantity and scenario is given in Fig. 7. The cross-sections show the flow behaviour at LB2 in the street canyon of Laura Bassi St.

Fig. 7a_1, a_2 show the wind-speed magnitude (colours) and circulation (streamlines). Note that QUIC-URB does not account for turbulent diffusion through a momentum equation. These approximation causes the circulation streamlines to form sharp edges in the vicinity of solid boundaries. The presence of trees in Fig. 7a_1 modifies the wind-speed magnitude driving a wave-like motion, propagating upwards from the tree tops. This behaviour is a consequence of the wind-speed reduction exerted by the parametrised drag force from the tree on the mean flow, while the propagation is due to mass conservation. The wavelike motion can either be a pressure-driven wave or a wake generated by the collision between the flow and the trees. Either way, the model's mass conservation sustains this wave-like motion and allows it to propagate vertically, generating a column of slower wind speed with respect to the surroundings.

The flow circulation is also modified by the presence of trees. In the No-Tree canyon, the flow is separated into two regions: a region with a single weak vortex motion at the surface and a recirculation zone immediately downwind of the leeward building with vertical velocity vectors pointing toward the rooftop. The trees destroy this circulation, breaking the swirling motion into two smaller eddies, a primary eddy in the middle of the street and a secondary one at the foot of the windward wall (see Fig. 7a_1). This secondary eddy creates a recirculation zone at pedestrian level, driving a stagnant region that could potentially decrease the canyon ventilation. Conversely, the primary eddy extends vertically, enhancing the street ventilation. The recirculation zone at the leeward wall is completely destroyed.

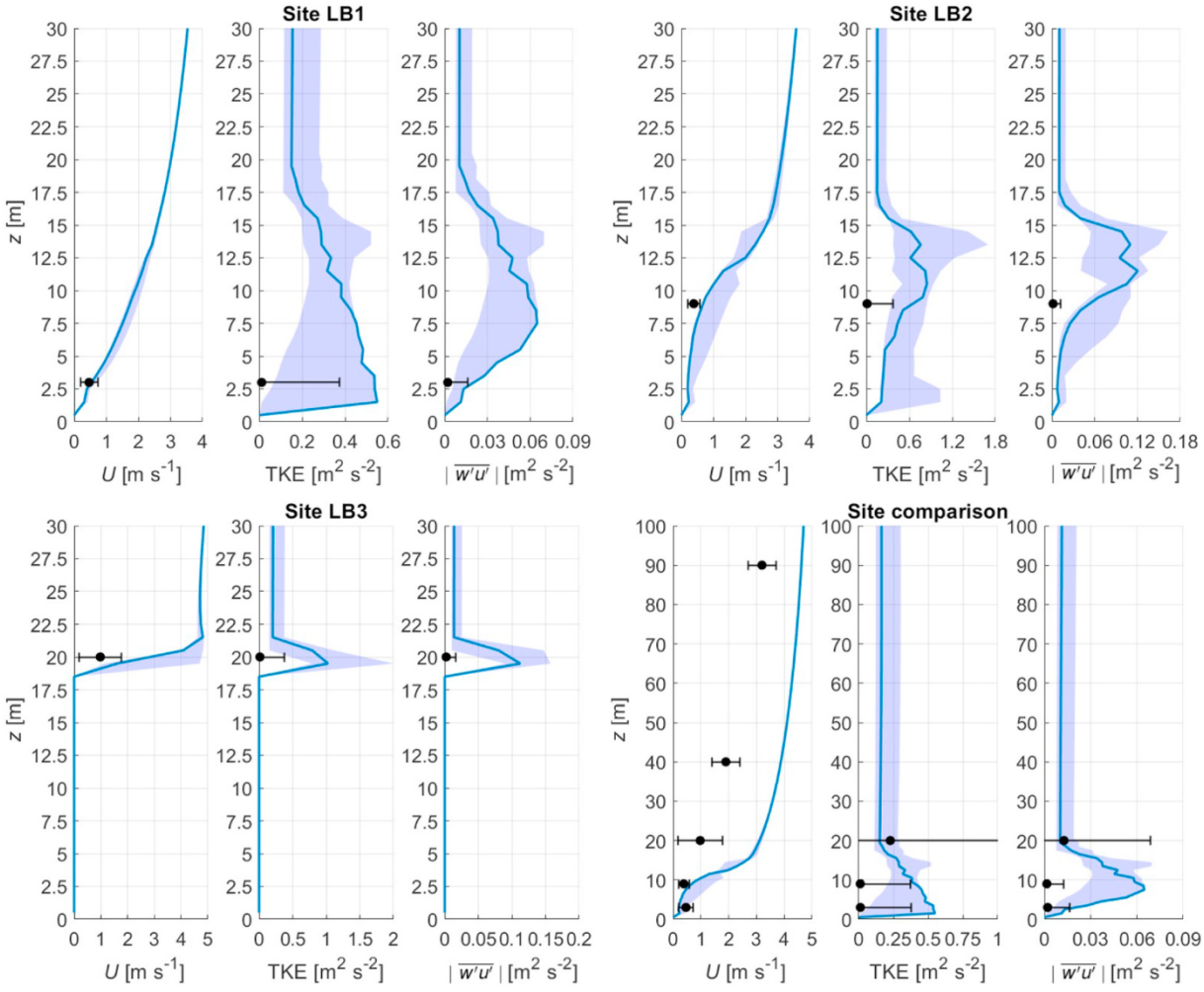

Fig. 6. Same as Fig. 3 but for the south parallel wind direction ensemble. The blue profile represents the 180° wind direction to the canyon orientation. (For interpretation of the references to colour in this figure legend, the reader is referred to the Web version of this article.)

Scaling directly with the mean flow intensity, TKE and $|\overline{w'u'}|$ are also modified by the presence of trees (refer to Fig. 7b_1, b_2 for TKE and to Fig. 7c_1 ,c_2 for $|\overline{w'u'}|$). Within the street canyon, the overall effect of vegetation is to decrease the homogeneity and modify the TKE pattern. In the No-Tree case (see Fig. 7b_2), the TKE is maximum at the building rooftops, protruding from the top edge of the leeward wall towards the canyon centre. A decrease in TKE is observed from the leeward to the windward wall, where TKE is nearly zero. Introducing vegetation into the canopy (see Fig. 7b_1) changes the structure as the trees create patches of different TKE intensity. TKE is observed to increase at the tree tops and bottoms, where the flow field is mostly modified by the enhanced pressure gradient (which results from the parametrised velocity field), and in general in the upper part of the canyon. Conversely, TKE decreases above the canopy, as a consequence of wind-speed reduction and on the windward rooftop, causing potential turbulence energy reduction in the downwind canopy or wake region.

The impact of trees on the turbulent kinematic momentum flux is similar to what was observed for the TKE, but limited to the rooftop interface. The No-Tree case (displayed in Fig. 7c_2) shows weak levels of $|\overline{w'u'}|$ within the canopy, despite an observed mean flow penetration. Homogeneous mixing and small gradients, mostly at the canyon-top interface, regulate the turbulent transport and potential canyon ventilation. As observed for TKE, the flux intensity increases at the tree tops, and decreases above the canopy and in the downwind building rooftop region (see Fig. 7c_1). Nevertheless, the small flux penetration observed in the No-tree case towards the leeward wall is missing as the trees break the flow at the canyon top.

The observed differences between the Tree and No-Tree cases in the street-canyon wind fields are in good agreement with recent CFD studies validated with datasets from laboratory experiments. Specifically, the persistence of the main vortex has been observed within a vegetative canyon [1,12], as an almost negligible wind-speed reduction in the lower part of the canopy [56]. Other observed characteristic of a vegetated canopy is the presence of recirculation vortex at pedestrian level [10]. Conversely, the current turbulent fields are found to be more largely modified by the presence of vegetation with respect to recent studies (e.g. Ref. [12], where the impact of trees results in an overall TKE reduction.

4.1. Tree and No-Tree cases distributions

The role of trees in the neighbourhood surrounding the Laura Bassi St. reference street canyon is investigated using a probability-distribution analysis. The investigation aims to describe the impact of trees in different vertical layers within and above the canopy. Four layers (i.e. ground, mid-canyon, rooftop, and roughness layers) have been defined to assess representative areas in real environments. The ground layer accounts for the portion of the canopy between the surface ($z_i = 1.5$ m $\approx z_0$) and $z_f = 4.5$ m, the atmospheric volume occupied by the tree trunks. The mid-canyon layer identifies the atmospheric volume where the lower half of the tree crowns is present, at heights included between $z_i = 5.5$ m and $z_f = 9.5$ m.

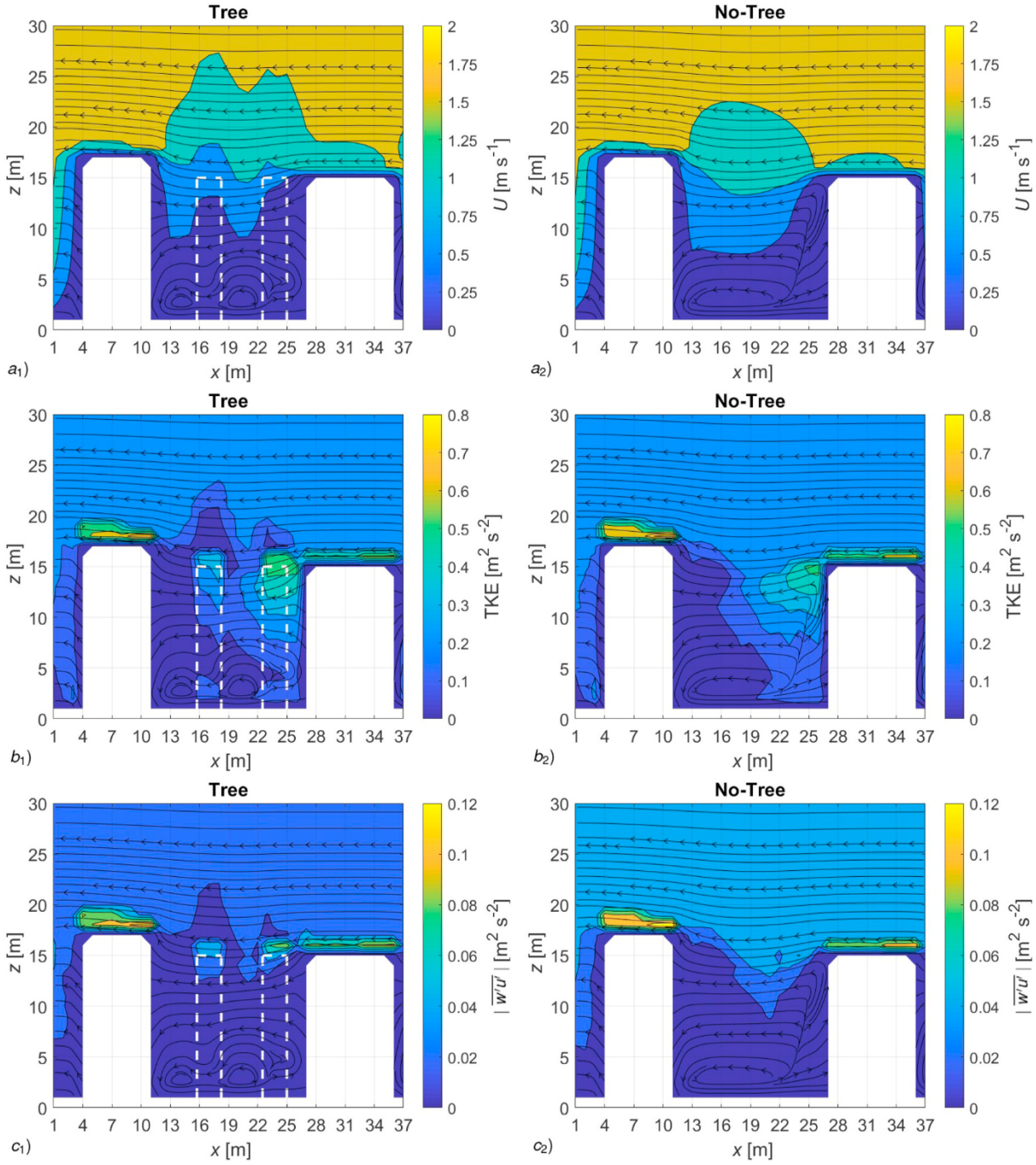

Fig. 7. Cross-sections in the Laura Bassi St. canyon at the location of the LB2 site. From top to bottom the colour maps represent wind speed (a), TKE (b) and turbulent kinematic momentum flux (c). Subscript 1 of panel identifiers refers to the Tree case, subscript 2 to the No-Tree one. Trees are represented as withe dashed rectangles. Streamlines represent the mean flow circulation. (For interpretation of the references to colour in this figure legend, the reader is referred to the Web version of this article.)

The interface between the canopy and urban boundary layer is identified as the rooftop layer, including the upper portion of the tree crowns, and ranges between $z_i = 10.5$ m and $z_f = 14.5$ m. A final layer corresponding to the approximate location of the roughness sublayer is located between $z_i = 15.5$ m and $z_f = 20.5$ m.

In this section, we continue to investigate the impact of vegetation using the Tree and No-Tree case scenarios. Changing the number of trees in the domain modifies the area density coefficients and the aerodynamic roughness length according to Table 2. From the simulation results, we computed normalised probability distributions for each layer and assessed the impact of trees on the mean wind speed, TKE and turbulent kinematic momentum flux (see Fig. 8). The green and the blue colours represent the No-Tree and Tree cases, respectively. Note that the scale of the abscissas are not the same for the rooftop-layer and roughness-layer distributions.

The general trend of the data indicates a shift in the peak of the distribution to the left (toward lower values) for the Tree case compared to the No-Tree case for all quantities analysed. This effect is more evident at the interface and outside the canopy layer, where the top of the tree crowns enhances the local roughness modifying the velocity and turbulence fields. In contrast, in the ground layer, differences are small because trees are not the predominant factor determining the

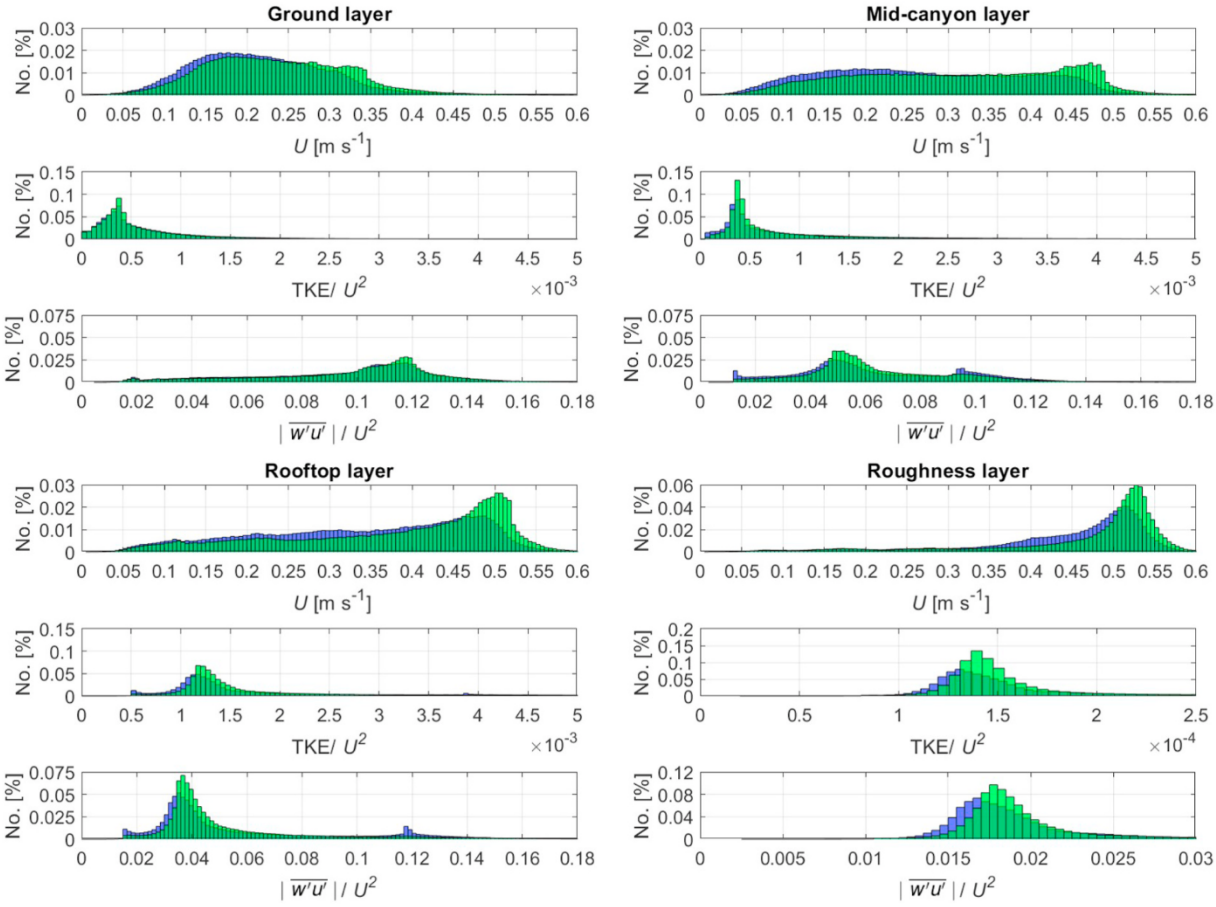

Fig. 8. Normalised probability distributions of mean wind speed, turbulence kinetic energy and turbulent kinematic momentum flux at (top left) ground, (top right) mid-canyon, (bottom left) rooftop and (bottom right) roughness sublayers respectively. Turbulence-related quantities are normalised over the squared mean wind speed at the corresponding layer. The blue distributions represent the Tree case and the green distributions are for the No-Tree case. (For interpretation of the references to colour in this figure legend, the reader is referred to the Web version of this article.)

ventilation. Building constraints also play a major role in the mid-canyon layer where the impact of the tree crown was expected to be maximum. Wind speed distributions inside the canopy are wide, accounting for a multitude of possible interactions between the varying and differently oriented morphology of the canopy. At the interface and especially in the roughness layer, the wind-speed distributions are more peaked around the respective modes, due to the increased homogeneity of the flow. As expected, the mean flow velocity is reduced by the presence of trees. Turbulence-related quantities do not have such stark tendencies. An increase of both TKE and momentum transport for the No-Tree case is observed in the roughness layer, where the overall effect of the wind speed is the enhancement of mechanical turbulence production. This behaviour is also found in the rooftop layer for the TKE, but momentum transport shows both increasing and decreasing effects. The momentum transport in the Tree case distribution is bi-modal, where a larger maximum is observed at $|\overline{w'u'}|/U^2 \approx 0.035$ and a smaller one is located at $|\overline{w'u'}|/U^2 \approx 0.11$. The distribution of the No-Tree case does not present this bi-modal behaviour, rather there is a single more frequent mode centred at $|\overline{w'u'}|/U^2 \approx 0.038$ with a long right tail. Therefore, in the No-Tree case, the first $|\overline{w'u'}|/U^2$ maximum is enhanced, but the impact of the second is totally lost. This same behaviour is also observed at the mid-canyon layer, despite the fact that the distribution differences between Tree and No-Tree cases are smaller. In the ground layer, both turbulence-related distributions show no significant differences between the two cases.

4.2. Domain discretisation and area fraction coefficient analysis

The vertical dashed black lines are placed at the threshold $\lambda_{p,f} = 0.225$.

Trees in the canopy layer modify the morphological parameters by introducing porous obstacles that cause a heterogeneous distribution of roughness elements. To better account for this effect, we have explicitly included vegetation elements within the urban morphology by modifying the area fraction coefficients (see Sect. 2.2.2). We hypothesise that the variation of the morphological parameters impact the mean flow and turbulence by changing the complexity of the urban environment. To quantify this impact, we divided the domain into squared sub-domains of constant plan area (length $l = 250$ m), inside of which we have computed the morphological parameters λ_p and λ_f with and without the vegetation.

Wind speed, TKE and turbulent kinematic momentum flux are displayed as function of the morphological parameters for each layer defined in Sect. 4.1 with the same input conditions applied in Sect. 3.1. Results are shown in Figs. 9–11, where wind speed, TKE and turbulent kinematic momentum flux are bin-averaged over a bin width of 0.01 units for λ_p and λ_f, each quantity displayed within the complete minimum-maximum range in each bin. Wind speeds in each layer show similar behaviours in the Tree and No-Tree cases (see Fig. 9). The wind speeds are affected by λ_f, which decrease as λ_f increases. This behaviour is particularly evident when $\lambda_f > 0.225$. Below this threshold, the tendency of wind speed becomes more independent of the morphology since the obstacle density is too small to substantially affect the mean

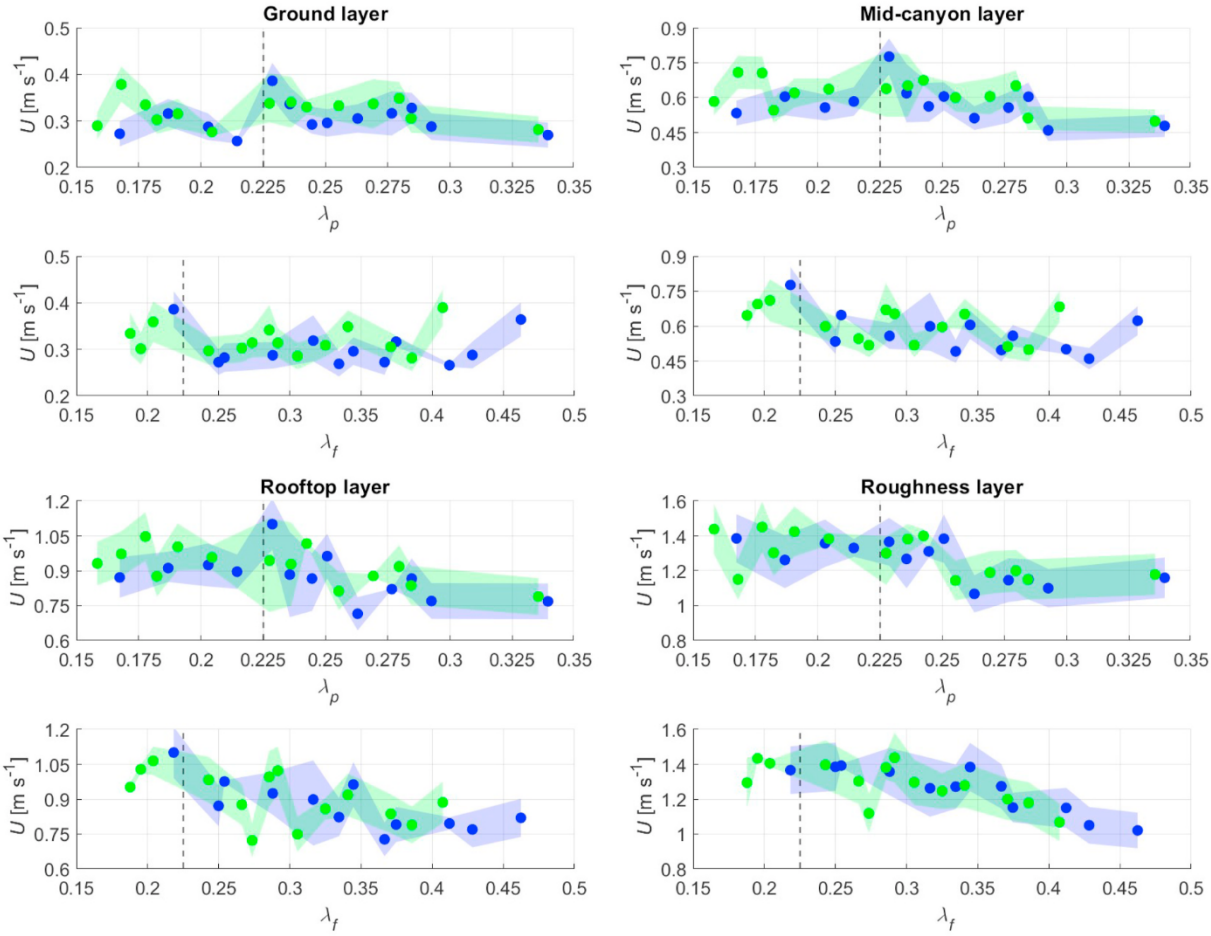

Fig. 9. Wind speed as a function of the planar (λ_p) and frontal (λ_f) area coefficients retrieved at ground (top left), mid-canyon (top right), rooftop (bottom left) and roughness (bottom right) layers respectively. The blue circles refer to the Tree case, the green ones to the No-Tree case. Each dot represents a bin-averaged wind speed with bin widths of 0.01 for λ_p and λ_f. The shaded areas define the complete range of the velocity data in each bin. (For interpretation of the references to colour in this figure legend, the reader is referred to the Web version of this article.)

flow. The only exception to this is in the ground layer where the wind speed is randomly distributed over the range of λ_f values. The wind speed appears to be more independent of λ_p, especially inside the canopy. In the rooftop and roughness layers, wind speed slightly decreases as λ_p increases. As shown in Sect. 4.1, wind speeds in the No-Tree case are larger than in the Tree case. In the ground and mid-canyon layers, the wind speed is again randomly distributed over λ_p. This anomalous behaviour might be a consequence of flow channelling. Not surprisingly, the presence of trees reduces the overall wind speed as well as the velocity gradients, but it does not consistently change in response to modifications of the morphology.

The normalised turbulence kinetic energy TKE/ U^2 in Fig. 10 show two well defined regimes shared by both morphological coefficients. When $\mathrm{TKE}/U^2 \leq 0.225$, the turbulence kinetic energy is independent of the morphology coefficients, as it was for the wind speeds. Above this threshold, TKE/U^2 rapidly increases as the coefficients increase. This second tendency is particularly evident in the Tree case in the rooftop and roughness layers, where the spread of the distribution seems to increase with the increasing λ_p and λ_f (as displayed in the bottom right and bottom left panels of Fig. 8). In the ground and mid-canyon layers of the Tree case, a certain imbalance is observed at $\lambda_f > 0.4$, where TKE destruction seems to overcome its production.

Nevertheless, this behaviour at the canyon surface remains poorly supported due to a lack of data in this range.

The normalised turbulent kinematic momentum fluxes $|\overline{w'u'}|/\ U^2$ approximately follow the same behaviour observed for the TKE, but their tendencies are less defined in some of the layers. Well-defined increasing trends are found for the Tree case where $|\overline{w'u'}|/U^2$ is function of λ_f in the mid-canyon and rooftop layers, and $|\overline{w'u'}|/U^2$ also increases with λ_p in the same layers when $\lambda_p \geq 0.225$. The No-Tree cases display an increasing tendency, but the strong oscillations perturb these trends, especially within the canopy. In the ground and roughness layers the tendencies are even less defined. In the first case, $|\overline{w'u'}|/U^2$ seems independent of both morphology parameters. In the roughness layer, fluxes are almost constant until both morphology parameters reach 0.225, then $|\overline{w'u'}|/U^2$ starts oscillating as λ_f increases, while it decreases as λ_p increases after a strong discontinuity has brought the fluxes close to their maximum value. Finally, the contribution of morphology on $|\overline{w'u'}|/U^2$ seems to increase in the layers where the tree crowns are located, but this behaviour does not apply either to the atmosphere above nor the ground layer.

To summarise, the overall impact of the modifications to canopy morphology (through vegetation density variation) on the mean flow and turbulence fields is small compared to the constraint imposed by buildings or other solid obstacles.

5. Summary and conclusions

The QUIC Dispersion Modeling System has been evaluated on a real vegetated urban neighbourhood (1000 m × 1300 m) within the city of Bologna, Italy, using the results from an experimental field campaign. Model validation in real urban canopies is always challenging due to the

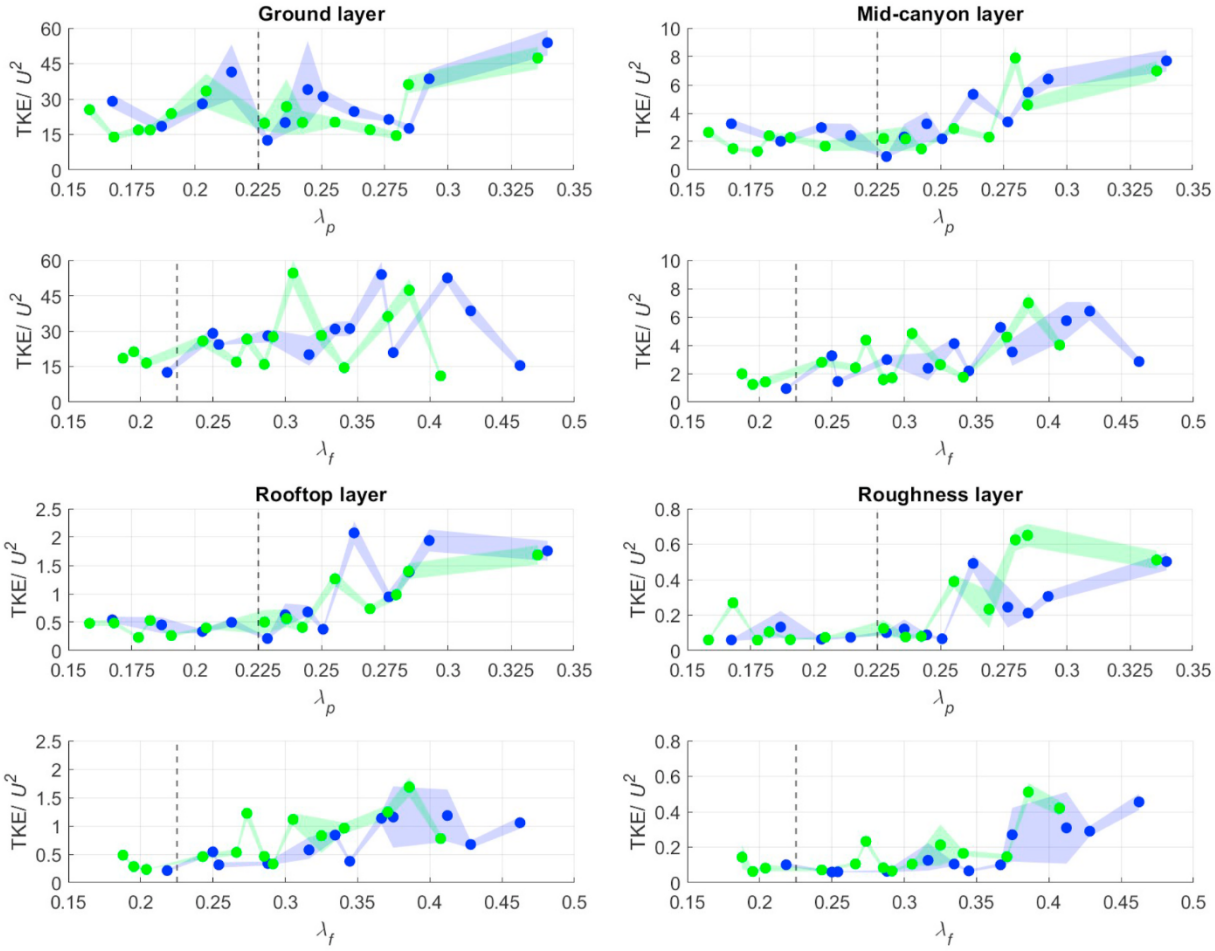

Fig. 10. Same as Fig. 9 but for for the normalised turbulence kinetic energy, TKE/U^2.

complex flow-field interactions in real and uncontrolled environments. Nevertheless, research and operational models are now able to represent atmospheric processes at finer resolutions, continuously improving the simulated results. In this context, QUIC has been shown to be a light-weight, easy-to-use numerical solver that is fast running and produces good results. The scope of this work was to test QUIC on a real European-style urban neighbourhood characterised by a network of narrow street canyons each flanked by two lines of deciduous trees. QUIC simulations have been validated using a dataset taken in Bologna during summer 2017 as part of the iSCAPE field campaign involving a street canyon (Laura Bassi St.) within the simulated domain.

Validation was performed for different incident wind directions. Specifically, wind directions that were perpendicular and parallel to the Laura Bassi St. orientation were considered. We implemented a methodology to maximise the comparability between the simulations and measurements. First, wind-direction ranges (or sectors) were defined. Within each sector, the wind direction is assumed constant. Second, steady-state periods were identified using the main flow characteristics in each sector to evaluate time-averages and standard deviations of the measurements. Third, QUIC's input conditions were defined for each sector to simulate these steady-state periods. Finally, simulation ensembles were generated for each sector, where the input conditions were kept constant apart from the wind direction, which could span the whole interval of a sector. This method was then applied to the investigations within this study. The simulation validation exercise yielded an overall good agreement with the measured mean flow and turbulence data, with the distribution of ensembles overlapping the variability in the measurements. Near-neutral conditions and perpendicular wind directions have been found to be better captured by the model, even though the presence of trees creates very local flow modifications, which are not fully resolved in the simulations. Weakly unstable conditions and thermal stratification decrease the quality of the simulated results, which still compare well to the data.

The role of trees in the urban canopy was addressed by comparing the numerical simulation results for the real-case scenario with a hypothetical case where trees were removed from the domain. A qualitative comparison between the reference street canyon cross-section showed that trees are found to substantially modify the flow circulation and intensity. The flow is forced into a wavelike motion propagating above the canopy and decreasing its speed. The canopy vortex is broken into smaller eddies, generating a recirculation zone at the foot of the windward wall. This feature could negatively impact local air quality. Trees are also found to increase the turbulence-field heterogeneity and to enhance the turbulence intensity at the canyon interface, potentially favouring canopy ventilation. The role of trees in the neighbourhood of Laura Bassi St. was addressed using a probability-distribution analysis. Mean wind speed, turbulence kinetic energy and turbulent kinematic momentum flux were obtained in different atmospheric layers and for the vegetated and the non-vegetated scenarios. The results show that the blocking effect of the trees dominates both mean-flow and turbulence fields.

Finally, the impact of morphology on the mean flow and turbulence fields was evaluated for the vegetated and non-vegetated scenarios. Not surprisingly, the mean flow and turbulence fields are sensitive to the density of the obstacles (buildings or trees). Specifically, two regimes have been identified, discriminated by a threshold in the area fraction

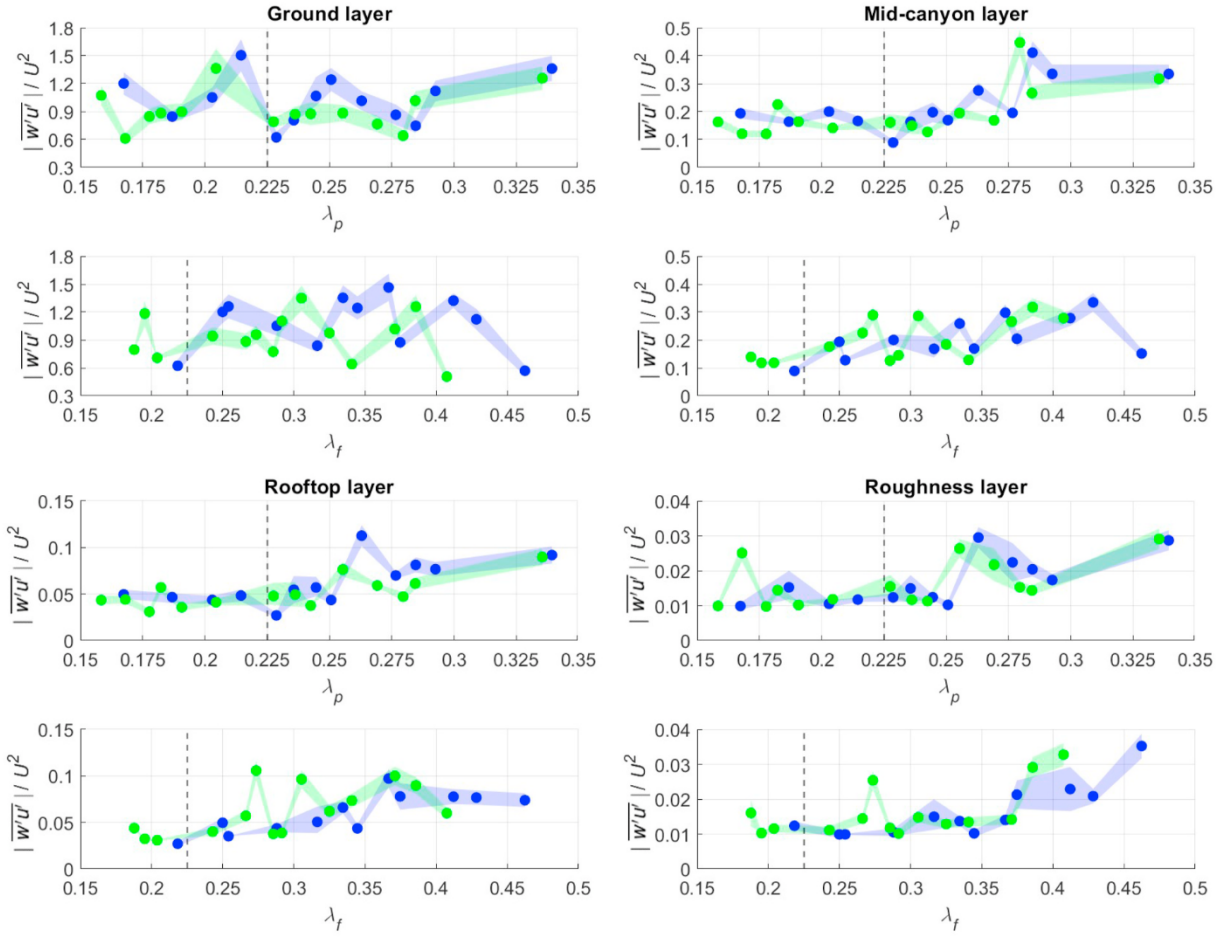

Fig. 11. Same as Fig. 9 but for the normalised turbulent kinematic momentum flux $|\overline{w'u'}|/U^2$.

coefficients. When $\lambda_{f,p} < 0.225$, both mean flow and turbulence fields are independent of obstacle density. Conversely, when $\lambda_{f,p} \geq 0.225$, the flow speed is reduced by the increasing obstacle density, while turbulence production dominates the destruction. This threshold was observed throughout the domain within different atmospheric layers, suggesting that the two morphological regimes exist throughout the surface layer. Finally, the morphology analysis has revealed the limited impact of vegetation compared to the impact of the building density.

To perform the morphology investigation, we have adopted the formalism introduced by Ref. [50] to explicitly represent the presence of vegetation in the area fraction coefficients. Even though this formalism for including vegetation within the morphology has been shown to perform better than other methods [57], this is a first-time evaluation with QUIC. Nevertheless, the agreement found validating the model results with measurements suggests the rationality in the choice of the formalism. Further investigation may be required, where we suggest the use of complete CFD models and laboratory experiments to address the impact of the vegetation evaluation method.

Declaration of competing interest

The authors declare that they have no known competing financial interests or personal relationships that could have appeared to influence the work reported in this paper.

Acknowledgments

This research has been supported by the iSCAPE (Improving the Smart Control of Air Pollution in Europe) project funded by the European Community's H2020 Programme (H2020-SC5-04-2015) under the Grant Agreement No.689954. In addition, this work was supported by the National Science Foundation (Division of Chemical, Bioengineering, Environmental, and Transport Systems (CBET)) under grant 1512740.

The authors want to acknowledge all the academics, researchers, specialists and students from the Department of Physics and Astronomy and the Department of Industrial Engineering of the University of Bologna, the local Environmental Agency (ARPAE) and the National Research Council (CNR) for their great effort dedicated to the realisation of the experimental field campaign.

References

[1] C. Gromke, R. Buccolieri, S. Di Sabatino, B. Ruck, Dispersion study in a street canyon with tree planting by means of wind tunnel and numerical investigations - evaluation of CFD data with experimental data, Atmos. Environ. 42 (37) (2008) 8640–8650.

[2] T. Van Renterghem, D. Botteldooren, Numerical evaluation of tree canopy shape near noise barriers to improve downwind shielding, J. Acoust. Soc. Am. 123 (2) (2008) 648–657.

[3] R. Buccolieri, S.M. Salim, L.S. Leo, S. Di Sabatino, A. Chan, P. Ielpo, G. de Gennaro, C. Gromke, Analysis of local scale tree-atmosphere interaction on pollutant concentration in idealized street canyons and application to a real urban junction, Atmos. Environ. 45 (9) (2011) 1702–1713.

[4] A. Jeanjean, R. Buccolieri, J. Eddy, P. Monks, R. Leigh, Air quality affected by trees in real street canyons: the case of Marylebone neighbourhood in central London, Urban For. Urban Green. 22 (2017) 41–53.

[5] G.G. Katul, L. Mahrt, D. Poggi, C. Sanz, One- and two-equation models for canopy turbulence, Boundary-Layer Meteorol. 113 (2004) 81–109.

[6] C. Gromke, B. Blocken, W. Janssen, B. Merema, T. van Hooff, H. Timmermans, CFD analysis of transpirational cooling by vegetation: case study for specific meteorological conditions during a heat wave in Arnhem, Netherlands, Build. Environ. 83 (2015) 11–26.

[7] R. Buccolieri, A.P.R. Jeanjean, E. Gatto, R.J. Leigh, The impact of trees on street ventilation, NOx and PM2.5 concentrations across heights in Marylebone Rd street canyon, central London, Sustain. Cities Soc. 41 (2018) 227–241.

[8] S. Rafael, B. Vicente, V. Rodrigues, A.I. Miranda, C. Borrego, M. Lopes, Impacts of green infrastructures on aerodynamic flow and air quality in Porto's urban area, Atmos. Environ. 190 (2018) 317–330.

[9] Q. Li, Z.H. Wang, Large-eddy simulation of the impact of urban trees on momentum and heat fluxes, Agric. For. Meteorol. 255 (2018) 44–56.

[10] C. Gromke, B. Ruck, Influence of trees on the dispersion of pollutants in an urban street canyon-Experimental investigation of the flow and concentration field, Atmos. Environ. 41 (16) (2007) 3287–3302.

[11] C. Gromke, B. Ruck, On the impact of trees on dispersion processes of traffic emissions in street canyons, Boundary-Layer Meteorol. 131 (1) (2009) 19–34.

[12] R. Buccolieri, C. Gromke, S. Di Sabatino, B. Ruck, Aerodynamic effects of trees on pollutant concentration in street canyons, Sci. Total Environ. 407 (19) (2009) 5247–5256.

[13] M. Moradpour, H. Afshin, B. Farhanieh, A numerical investigation of reactive air pollutant dispersion in urban street canyons with tree planting, Atmos Pollut. Res. 8 (2017) 253–266.

[14] P.E.J. Vos, B. Maiheu, J. Vankerkom, S. Janssen, Improving local air quality in cities: to tree or not to tree? Environ. Poll. 183 (2013) 113–122.

[15] D.J. Nowak, S. Hirabayashi, A. Bodine, R. Hoehn, Modeled PM2.5 removal by trees in ten U.S. cities and associated health effects, Environ. Poll. 178 (2013) 395–402.

[16] B. Hong, H. Qin, B. Lin, Prediction of wind environment and indoor/outdoor relationships for PM2.5 in different building-tree grouping patterns, Atmosphere 9 (2) (2018).

[17] A. Hagishima, K. Narita, J. Tanimoto, Field experiment on transpiration from isolated urban plants, Hydrol. Proc. 21 (9) (2007) 1217–1222.

[18] S. Di Sabatino, R. Buccolieri, G. Pappaccogli, L.S. Leo, The effects of trees on micrometeorology in a real street canyon: consequences for local air quality, Int. J. Environ. Pollut. 58 (2015) 100–111.

[19] J.H. Amorim, V. Rodrigues, R. Tavares, J. Valente, C. Borrego, CFD modelling of the aerodynamic effect of trees on urban air pollution dispersion, Sci. Total Environ. 461 (2013) 541–551.

[20] J. Santiago, R. Buccolieri, E. Rivas, B. Sanchez, A. Martilli, E. Gatto, F. Martín, On the impact of trees on ventilation in a real street in pamplona, Spain, Atmosphere 10 (11) (2019) 697.

[21] M.G. Giometto, A. Christen, P.E. Egli, M.F. Schmid, R.T. Tooke, N.C. Coops, M. B. Parlange, Effects of trees on mean wind, turbulence and momentum exchange within and above a real urban environment, Adv. Water Resour. 106 (2017) 154–168.

[22] R. Buccolieri, J. Santiago, E. Rivas, B. Sanchez, Review on urban tree modelling in CFD simulations: aerodynamic, deposition and thermal effects, Urban For. Urban Green. 31 (2018) 212–220.

[23] M. Balczó, C. Gromke, B. Ruck, Numerical modeling of flow and pollutant dispersion in street canyons with tree planting, Meteorol. Z. 18 (2009) 197–206.

[24] J. Liu, J.M. Chen, M. Novak, E - ε Modelling of turbulent air flow downwind of a model forest edge, Boundary-Layer Meteorol. 77 (1996) 21–44.

[25] M.J. Brown, A.A. Gowardhan, M.A. Nelson, M.D. Williams, E.R. Pardyjak, QUIC transport and dispersion modelling of two releases from the Joint Urban 2003 field experiment, Int. J. Environ. Pollut. 52 (3/4) (2013) 263.

[26] M.D. Williams, M.J. Brown, D. Boswell, B. Singh, E.R. Pardyjak, Ame Meteor Soc, Testing of the QUIC-PLUME model with wind-tunnel measurements for a high-rise building, in: Testing of the QUIC-PLUME Model with Wind-Tunnel Measurements for a High-Rise Building, 2004, p. 10.

[27] E.R. Pardyjak, S.O. Speckart, F. Yin, J.M. Veranth, Near source deposition of vehicle generated fugitive dust on vegetation and buildings: model development and theory, Atmos. Environ. 42 (26) (2008) 6442–6452.

[28] B. Singh, B.S. Hansen, M.J. Brown, E.R. Pardyjak, Evaluation of the QUIC-URB fast response urban wind model for a cubical building array and wide building street canyon, Environ. Fluid Mech. 8 (2008) 281–312.

[29] R. Röckle, Bestimmung der Strömungsverhältnisse im Bereich komplexer Bebauungsstrukturen. na, 1990.

[30] H. Kaplan, N. Dinar, A Lagrangian dispersion model for calculating concentration distribution within a built-up domain, Atmos. Environ. 30 (24) (1996) 4197–4207.

[31] R.M. Cionco, A mathematical model for air flow in vegetative canopy, J. Appl. Meteorol. 4 (1965) 517–522.

[32] B. Singh, E.R. Pardyjak, A. Norgren, P. Willemsen, Accelerating urban fast response Lagrangian dispersion simulations using inexpensive graphics processor parallelism, Environ. Model. Software 26 (6) (2011) 739–750.

[33] M.D. Williams, M.A. Nelson, M.J. Brown, Condensed Quic-Plume Theory Guide for Quic-Fst. Tech. rep., Los Alamos National Lab.(LANL), 2019. Los Alamos, NM (United States).

[34] A.A. Gowardhan, E.R. Pardyjak, I. Senocak, M.J. Brown, A CFD-based wind solver for an urban fast response transport and dispersion model, Environ. Fluid Mech. 11 (2011) 439–464.

[35] M. Neophytou, A. Gowardhan, M. Brown, An inter-comparison of three urban wind models using Oklahoma City Joint Urban 2003 wind field measurements, J. Wind Eng. Ind. Aerod. 99 (4) (2011) 357–368.

[36] A.N. Hayati, R. Stoll, J.J. Kim, T. Harman, M.A. Nelson, M.J. Brown, E.R. Pardyjak, M.J. Brown, Comprehensive evaluation of fast-response, Reynolds-averaged Navier-Stokes, and large-eddy simulation methods against high-spatial-resolution wind-tunnel data in step-down street canyons, Boundary-Layer Meteorol. 164 (2017) 217–247.

[37] S. Hanna, J. White, J. Trolier, R. Vernot, M. Brown, A. Gowardhan, H. Kaplan, Y. Alexander, J. Moussafir, Y. Wang, C. Williamson, J. Hannan, E. Hendrick, Comparisons of JU2003 observations with four diagnostic urban wind flow and Lagrangian particle dispersion models, Atmos. Environ. 45 (24) (2011) 4073–4081.

[38] A.K. Kochanski, E.R. Pardyjak, R. Stoll, A. Gowardhan, M.J. Brown, W. J. Steenburgh, One-way coupling of the WRF-QUIC Urban dispersion modeling system, J. Appl. Meteor. Clim. 54 (10) (2015) 2119–2139.

[39] M.A. Nelson, M.J. Brown, S.A. Halverson, P.E. Bieringer, A. Annunzio, G. Bieberbach, S. Meech, M.A. Nelson, A case study of the weather research and forecasting model applied to the joint urban 2003 tracer field experiment. Part 2: gas tracer dispersion, Boundary-Layer Meteorol. 161 (2016) 461–490.

[40] P. Girard, D.F. Nadeau, E.R. Pardyjak, M. Overby, P. Willemsen, R. Stoll, B. N. Bailey, M.B. Parlange, Evaluation of the QUIC-URB wind solver and QESRadiant radiation-transfer model using a dense array of urban meteorological observations, Urban Clim. 24 (2018) 657–674.

[41] S. Di Sabatino, L.S. Leo, R. Cataldo, R.E. Britter, Construction of digital elevation models for a southern European city and a comparative morphological analysis with respect to northern European and north American cities, J. Appl. Meteorol. Clim. 49 (2010) 1377–1396.

[42] F. Barbano, E. Brattich, S. Di Sabatino, Characteristic scales for turbulent exchange processes in a real urban canopy, Boundary-Layer Meteorol. 1–24 (2020).

[43] M. Aubinet, T. Vesala, D. Papale, Eddy Covariance: a Practical Guide to Measurement and Data Analysis, Springer Science & Business Media, 2012.

[44] J. Højstrup, Statistical data screening procedure, Meas. Sci. Technol. 4 (1993) 153–157.

[45] D. Vickers, L. Mahrt, Quality Control and flux sampling problems for tower and aircraft data, J. Atmos. Ocean. Technol. 14 (1997).

[46] H.P. Schmid, C.S.B. Grimmond, F. Cropley, B. Offerle, H. Su, Measurements of CO2 and energy fluxes over a mixed hardwood forest in the mid-western United States, Agric. For. Meteorol. 103 (4) (2000) 357–374.

[47] R. McMillen, An eddy correlation technique with extended applicability to non-simple terrain, Boundary-Layer Meteorol. 43 (3) (1988) 231–245.

[48] A.N. Hayati, R. Stoll, E.R. Pardyjak, T. Harman, J.J. Kim, Comparative metrics for computational approaches in non-uniform street-canyon flows, Build. Environ. 158 (2019) 16–27.

[49] R.W. Macdonald, R.F. Griffiths, D.J. Hall, An improved method for the estimation of surface roughness of obstacle arrays, Atmos. Environ. 32 (11) (1998) 1857–1864.

[50] W.C. Kent, S. Grimmond, D. Gatey, Aerodynamic roughness parameters in cities: inclusion of vegetation, J. Wind Eng. Ind. Aerod. 169 (2017) 168–176.

[51] R.M. Cionco, A wind-profile index for canopy flow, Boundary-Layer Meteorol. 3 (2) (1972) 255–263.

[52] D. Guan, Y. Zhang, T. Zhu, A wind-tunnel study of windbreak drag, Agric. For. Meteorol. 118 (1–2) (2003) 75–84.

[53] R.W. Macdonald, Modelling the mean velocity profile in the urban canopy layer, Boundary-Layer Meteorol. 97 (2000) 25–45.

[54] C. Ratti, S. Di Sabatino, R. Britter, M. Brown, F. Caton, S. Burian, Analysis of 3-D urban databases with respect to pollutant dispersion for a number of European and American cities, Water Air Soil Pollut. 2 (2002) 459–469.

[55] F. Barbano, Characterization of Turbulent Exchange Processes in Real Urban Street Canyons with and without Vegetation, Ph.D. thesis, alma, 2020.

[56] M.H. Salim, K.H. Schlünzen, D. Grawe, Including trees in the numerical simulations of the wind flow in urban areas: should we care? J. Wind Eng. Ind. Aerod. 144 (2015) 84–95.

[57] C.W. Kent, K. Lee, H.C. Ward, J. Hong, J. Hong, D. Gatey, S. Grimmond, Aerodynamic roughness variation with vegetation: analysis in a suburban neighbourhood and a city park, Urban Ecosyst. 21 (2018) 227–243.

[58] A.A. Gowardhan, M.J. Brown, E.R. Pardyjak, Evaluation of a fast response pressure solver for flow around an isolated cube, Environ. Fluid Mech. 10 (2010) 311–328.

[59] C. Gromke, B. Blocken, Influence of avenue-trees on air quality at the urban neighborhood scale. Part I: quality assurance studies and turbulent Schmidt number analysis for RANS CFD simulations, Environ. Poll. 196 (2015) 214–223.